The evolution of red colour vision is linked to coordinated rhodopsin tuning in lycaenid butterflies

Marjorie A. Liénard[a,b,*], Gary D. Bernard[c], Andrew A. Allen[a], Jean-Marc Lassance[b], Siliang Song[b], Richard Rabideau Childers[b], Nanfang Yu[d], Dajia Ye[b], Adriana Stephenson[b], Wendy Valencia-Montoya[b], Shayla Salzman[b], Melissa R.L. Whitaker[b], Michael Calonje[e], Naomi E. Pierce[b,*]

[a] The Broad Institute of MIT and Harvard, Cambridge, MA 02142, USA.

[b] Department of Organismic and Evolutionary Biology and Museum of Comparative Zoology, Harvard University, Cambridge, MA 02138, USA.

[c] Department of Electrical & Computer Engineering, University of Washington, Seattle, WA, USA.

[d] Department of Applied Physics and Applied Mathematics, Columbia University, New York, NY 10027, USA

[e] Montgomery Botanical Center, 11901 Old Cutter Road, Miami, FL 33156, USA.

Present addresses:

Department of Biology, Lund University, Lund, Sweden (MAL), Department of Ecology and Evolutionary Biology, University of Michigan, 500 S. State Street, Ann Arbor, MI 48109, USA. (SiSo), Department of Biology, University of Pennsylvania, PA 19104, USA (DY); Gene therapy program, University of Pennsylvania, PA 19104, USA (AS); School of Integrative Plant Sciences, Section of Plant Biology, Cornell University, 502 Mann Library, Ithaca, NY 14853, USA (ShSa); Entomological Collection, Department of Environmental Systems Science, ETH Zürich, Zürich, Switzerland (MRLW)

[*]Corresponding authors:

Marjorie A. Liénard, Biology Department, Lund University, Sölvegatan 35B, 22362 Lund, Sweden, marjorie.lienard@biol.lu.se

Naomi E. Pierce, Department of Organismic and Evolutionary Biology, MCZ laboratories 4th floor, Harvard University, 26 Oxford Street, Cambridge, MA 02138, USA, npierce@oeb.harvard.edu

ORCIDs in alphabetical order by name:

GDB: 0000-0001-7460-5123, RRC: 0000-0002-7137-3192, JML: 0000-0002-3675-6956, MAL: 0000-0003-3193-3666, WVM: 0000-0001-9246-2330, NEP: 0000-0003-3366-1625, SSa: 0000-0001-6808-7542 MRLW: 0000-0002-8774-8518.

Classification

Biological Sciences, Evolution, Ecology/Molecular Biology

This PDF file includes:

Main Text, Figures 1 to 7, Supplementary appendix (Figures S1 to S5, datafiles S1-S2)

Abstract

Colour vision is largely mediated by changes in number, expression, and spectral properties of rhodopsins, but the genetic mechanisms underlying adaptive shifts in spectral sensitivity remain largely unexplored. Using *in vivo* photochemistry, optophysiology, and *in vitro* functional assays, we link variation in eye spectral sensitivity at long wavelengths to species-specific absorbance spectra for LW opsins in lycaenid butterflies. In addition to loci specifying an ancestral green-absorbing rhodopsin with maximum spectral sensitivity (λ_{max}) at 520-530 nm in *Callophrys sheridanii* and *Celastrina ladon,* we find a novel form of red-shifted LW rhodopsin at λ_{max} = 565-570 nm in *Arhopala japonica* and *Eumaeus atala.* Furthermore, we show that *Ca. sheridanii* and *Ce. ladon* exhibit a smaller bathochromic shift at BRh2 (480-489 nm), and with the ancestral LW rhodopsin, cannot perceive visible red light beyond 600 nm. In contrast, molecular variation at the LW opsin in *A. japonica* and *E. atala* is coordinated with tuning of the blue opsin that also shifts sensitivity to longer wavelengths enabling colour discrimination up to 617 nm. We then use *E. atala* as a model to examine the interplay between red and blue spectral sensitivity. Owing to blue duplicate expression, the spatial distribution of opsin mRNAs within an ommatidium defines an expanded retinal stochastic mosaic of at least six opsin-based photoreceptor classes. Our mutagenesis *in vitro* assays with BRh1 (λ_{max} = 435 nm) chimeric blue rhodopsins reveal four main residues contributing to the 65 nm bathochromic shift towards BRh2 (λ_{max} = 500 nm). Adaptations in this four-opsin visual system are relevant for discrimination of conspecific reflectance spectra in *E. atala*. Together, these findings illustrate how functional changes at multiple rhodopsins contribute to the evolution of a broader spectral sensitivity and adaptation in visual performance.

Keywords

molecular evolution, ecological adaptation, visual system/vision, rhodopsin, spectral sensitivity, insects, Lepidoptera

Significance Statement

Rhodopsins are photosensitive protein molecules that absorb specific wavelengths of incoming light and convey colour information in the visual system. We show that molecular evolution in a green insect opsin gene resulted in a shift in its maximal absorbance peak, enabling some lycaenid butterflies to use spectral energy of longer wavelengths (LW) to discriminate colours in the red spectrum better than relatives bearing ancestral green LW rhodopsins. Lycaenids also evolved a duplicate blue opsin

gene, and we illustrate an example where species equipped with red LW rhodopsins shifted their blue sensitivity peak to longer wavelengths due to changes in several blue-tuning residues that have evolved repeatedly in different insect lineages. We demonstrate how changes at multiple vision genes in the insect eye effectively create a coordinated mechanism expanding spectral sensitivity for visually guided behaviours such as selecting host plants and mates.

Introduction

Multiple studies have demonstrated the important contributions of gene duplication and protein-coding changes in the evolution of novelty in lineage-specific phenotypic traits (1-3). For instance, gene duplication combined with modifications leading to functional divergence has contributed to gene family expansion, ultimately increasing transcriptional and functional diversity across lineages (2, 4). Recent examples show that specialization of ancestral functions (5-7) or cooperation between encoded products of duplication (8) are common mechanisms resolving constraints in existing eukaryotic gene networks (9). Genomic segmental duplications have also been shown to promote repeated allelic fixation, linking adaptive duplicated loci to convergent evolutionary pathways (10).

However, structural, functional, or gene network constraints can impose evolutionary trade-offs if there is limited variation for alternative biochemically stable encoded products among duplicated loci within multigene families (9, 11). Characterizing the molecular patterns of evolution within multigene families, and identifying the functional role of mutations at lower taxonomic scales is needed to distinguish the multiple sources of molecular variation. This includes the relative roles of gene duplication, expression changes, protein sequence divergence and convergence, or cellular relocalization of encoded gene products that contribute to new or convergent phenotypes within lineages (2, 7, 8, 12, 13).

Opsins belong to a diverse multigene family of G protein-coupled receptors, offering a robust framework to study how molecular changes can ultimately cause changes in behaviour and favour diversification (14). Opsins bind to a small non-protein retinal moiety derived from vitamin A to form photosensitive rhodopsins and enable vision across animals (15-18). The evolution of vision across the animal kingdom has long been linked to independent opsin gene gains and losses (19-23), genetic variation across opsins (15, 24-26), and spectral tuning mutations within opsins (27, 28). These molecular mechanisms , together with alterations in visual regulatory networks (29), have been shown to contribute to rhodopsin adaptation and the diversification of spectral sensitivity phenotypes in insects (18, 30, 31) and vertebrates including fish, birds, bats and primates (32-36). Thus multiple levels of organization, including the evolutionary

diversification of opsin subfamilies, their functional properties and regulatory networks constitute the mechanistic basis for organisms to discriminate light sources of varying wavelengths and ultimately interpret them as colours, yet how multiple changes across opsin paralog repertoires impact spectral sensitivity at small taxonomic scales has been understudied.

The evolution of insect colour vision in particular shows how a complex sensory trait can play a central role in adaptations involving signalling and mate communication (18, 31, 37, 38). Whereas the ancestral repertoire of insects involved three types of light-absorbing rhodopsin genes: ultraviolet (UVRh, 350nm), blue (BRh, 440 nm) and green, also called long-wavelength (LWRh, 530nm) (18), today's genomes harbor smaller or larger rhodopsin repertoires with strong experimental evidence for repeated functional convergence toward UV, Blue and LW spectral sensitivities across lineages. For example, beetles lost their ancestral blue opsin gene 300 million years ago, and compensated for the loss of blue sensitivity via either UV or LW gene duplication across lineages (23, 39). Blue opsin duplications occurred independently in pierid and lycaenid butterflies (27, 30, 40-42); and extend photosensitivity into the UV/blue in *Heliconius* spp. with λ_{max} = 355 nm and 398 nm (21) and into the violet/blue, in *Pieris rapae* with λ_{max} = 420 and 450 nm (27). UV and LW duplications occurred in butterflies, hemipterans and dragonflies (20, 22, 26, 30, 43-45). In butterflies, LW opsin duplications have been identified in two papilionids, *Papilio xuthus* (31) and *Graphium sarpedon* (46) as well as a riodinid *(Apodemia mormo)* (20, 47), and contribute to extend spectral sensitivity into the far red.

Although duplicated LW opsins have never been detected in the families Nymphalidae, Pieridae or Lycaenidae (25, 40, 41), photoreceptor types with sensitivity peaks in the red have been identified in these groups (40, 41). This supports the hypothesis that additional mechanisms such as lateral filtering and/ or molecular variation of ancestral LW opsin genes also contribute to modify long-wavelength sensitivity.

For example, photostable lateral filtering pigments are relatively widespread across butterfly lineages (e.g. *Heliconius* (21)*, Papilio (45), Pieris* (48), *Colias erato* (49), and some moths (*Adoxophyes orana,* (50)*; Paysandisia archon* (51)). These pigments

105 act as long-pass filters, absorbing short wavelengths and pushing the sensitivity peak of
106 LW photoreceptors into the red, to create distinct spectral types that can contribute to
107 colour vision (19, 31, 40, 48, 52, 53). Lateral filtering can shift peak sensitivity to longer
108 wavelengths while reducing peak amplitude, but cannot *extend* photoreceptor sensitivity
109 into the far red beyond the exponentially decaying long-wavelength rhodopsin
110 absorbance spectrum (52). Molecular variation of ancestral LW opsin genes could
111 potentially extend photoreceptor sensitivity, but this mechanism has remained difficult to
112 disentangle from the effects of filtering granules using classical electrophysiological
113 approaches (31, 53, 54).

114 The molecular underpinnings of mammalian MWS/ LWS spectral tuning has
115 been studied using mutagenesis experiments and led to the identification of critical
116 amino acid replacements and their interactions at key residues (55, 56). Most
117 mammalian lineages possess long-wavelength sensitive (LWS) cone opsins that specify
118 Medium (M, λ_{max} 510-540 nm) and Long (L, λ_{max} > 540 nm) rhodopsins. In humans,
119 trichromatic vision is conferred through the use of Short (S, λ_{max} = 414 nm), and tandem
120 duplicate M (λ_{max} = 530 nm) and L (λ_{max} = 560 nm) cone rhodopsins (34), that collectively
121 allow us to discriminate longer wavelengths of light as green-red colours (57, 58). In
122 birds, tetrachromatic vision is based on two SWS cone opsins, together with a green M
123 opsin (λ_{max} = 497-514 nm) and a red-sensitive LWS opsin (λ_{max} = 543-571 nm) (reviewed
124 in 59). In insects, the evolution of red receptors occurred independently multiple times
125 (30) but the possible contribution of molecular variation to insect LW opsin gene
126 diversification has remained elusive, notably due to difficulties in expressing LW opsins
127 *in vitro* (27, 60, 61, but see 62). Red receptors are intriguingly very common in butterflies
128 compared to other insect groups such as bees or beetles (30), raising the possibility that
129 perception of longer wavelengths plays an important role in the context of foraging (31,
130 46, 63), oviposition (64, 65) and mate recognition (25) for species equipped with them.

131 Lycaenids comprise the second largest family of butterflies, representing almost
132 thirty percent of all species, and exhibiting considerable ecological and morphological
133 diversity (66, 67). Pioneering work showed that species of Lycaenidae in the genera
134 *Lycaena* and *Polyommatus* have expanded spectral sensitivity at long wavelengths, and
135 this has been postulated to arise from filtering pigments, modified opsins or both (19, 40,

41). Here, by combining physiological, molecular and functional approaches, we identify additional lycaenid species with red photoreceptors and elevated spectral sensitivity at long wavelengths, and show that their LW opsin locus specifies a novel type of LW rhodopsin with red-shifted maximal absorbance. We focus on the Atala hairstreak (*Eumaeus atala*) as a suitable model to show the interplay between regulatory and adaptive changes at multiple opsin loci in the evolution of red spectral sensitivity and link the evolution of finely tuned four-opsin vision to relevant visually guided behaviours in these butterflies.

Results

Hairstreak butterflies with elevated sensitivity at long wavelengths express red-shifted rhodopsin receptors

A photographic series at distinct elevations in the eye revealed dramatic differences in eyeshine colouration between two pairs of lycaenids (Fig. 1 insets and Fig. S1). The Spring Azure, *Celastrina ladon* (subfamily Polyommatinae) and Sheridan's green hairstreak, *Callophrys sheridanii* (subfamily Theclinae), present homogeneous green and orange eyeshine in their dorsal eyes at 30° elevation, with a relatively small number of red ommatidia (*Ce. ladon*, 5%; *Ca. sheridanii*, 16%) (Fig. S1A-B). By contrast, the Japanese Oakblue, *Arhopala japonica,* and the Atala Hairstreak, *Eumaeus atala* (both subfamily Theclinae), share high levels of saturated red eyeshine in the dorso-equatorial region, due at least in part to species-specific differences in rhodopsin content (Fig. 1, Fig. S1B).

We partially bleached eyeshine of *A. japonica* and *E. atala* using repeated white-light flashes to reveal two types of ommatidia. Some ommatidia were resistant to bleaching and maintained their red eyeshine owing to lateral filtering by cherry-red pigment granules located distally within the photoreceptor cells of those ommatidia. The rest of the ommatidia were bleached, suggesting the presence of red sensitive opsin-based photoreceptors in these two species (Fig. S1C).

To test for the presence of red sensitive receptors, we performed analyses of *in vivo* photochemical rhodopsin bleaching measurements of adult butterflies. These experiments revealed long wavelength (LW) spectral sensitivities in dark-adapted eyes of *A. japonica* with λ_{max} ± standard error at 571 ± 2.45 nm ($CI_{95\%}$ = 566 to 576 nm) (Fig. 1A) and *E. atala* with λ_{max} at 563 nm ± 0.9 nm ($CI_{95\%}$ = 561 to 566 nm), respectively (Fig. 1B). We found that the two other lycaenid species we studied, *Ca. sheridanii* and *Ce. ladon,* were difficult subjects for our *in vivo* methods. In *Ca. sheridanii,* a noisy difference spectra obtained by photochemistry provided an estimate at LW λ_{max} = 518 nm ± 3.7 nm for ($CI_{95\%}$ = 511 to 526 nm) (Fig. 1C). Similarly, in *Ce. ladon,* partial LW bleaches were not measurable due to low LW rhodopsin densities,.

174 We chose to examine in detail the *in vivo* and *in vitro* contributions of all
175 rhodopsin pigments in *E. atala*, a multi-brooded and abundant hairstreak butterfly
176 naturally occurring throughout the year in Florida (USA) (68). Unlike most lycaenids, *E.*
177 *atala* larvae are extreme specialist herbivores on New World cycads in the genus *Zamia*
178 and show an unusually bright aposematic colouration advertising toxins they sequester
179 from their hosts (69). Conversely, the adult is a striking velvety black butterfly with bright
180 blue and red colours on the wings and the abdomen (Fig. 1) and can collect nectar from
181 43 species across 20 plant families (69)

182 We first analyzed epi-microspectrophotometric difference spectra obtained after
183 intense ommatidial flashing from a series of interference filters, which in addition to
184 identifying R565 (LW rhodopsin, Fig. 1B) allowed us to narrow down a blue rhodopsin at
185 R440 (Fig. 2A). Optophysiology measurements confirmed that neither the R565 LW nor
186 the R440 blue sensitive rhodopsins could be responsible for the high sensitivity around
187 360 nm, which instead was due to UV-receptors (Fig. 2B, Table S2). Finally, a
188 densitometric analysis of male and female eyes (Fig 2C-D, Tables S3-S4), showed that
189 these physiological data are best fit using least-squares regression by a model in which
190 four rhodopsins are present in the eye with λ_{max} values matching the LWRh rhodopsin as
191 well as UVRh 360 nm, BRh1 441.3 nm ± 4.7 nm ($CI_{95\%}$ = 431.7 to 450.9 nm, Table S2)
192 and a second blue rhodopsin BRh2 494.2 ± 1.2 nm ($CI_{95\%}$ = 492 to 497 nm) (Fig. 2E-F,
193 Tables S3-4).

194

195 ***Red sensitivity is due to functional variation at long-wavelength opsin loci***

196 Transcriptomic mRNA profiling of *E. atala* yielded only a single LW opsin (Table
197 S6), which is in line with earlier molecular evidence showing that lycaenid species
198 possess one LW opsin gene (30, 40, 53). Accordingly, eye cDNA library screening using
199 degenerated oligonucleotide primers followed by RACE cDNA amplification led to the
200 characterization of single orthologous LW cDNA sequences in *Ce. ladon*, *Ca. sheridanii*
201 and *A. japonica* (Fig. 3). We optimized an *in vitro* HEKT293 cell culture assay to
202 reconstitute heterologous rhodopsin pigments (27, 61, 70, 71) by using a newly
203 engineered heterologous vector to increase expression levels, and improving purification

204 procedures to obtain higher yields of actively reconstituted LW rhodopsins. Our
205 expression cassette derives from the pcDNA5 plasmid and expresses coding opsin
206 sequences tagged with a C-terminal FLAG epitope under a strong CMV promoter.
207 Directly downstream the FLAG epitope, a short peptide linker plus a T2A cleavage
208 cassette enable co-transcription of a fused cytoplasmic fluorescent mRuby2 coding
209 sequence (Fig. 3A). This expression cassette proved to be efficient at detecting
210 monomeric units of ultraviolet, blue and long-wavelength (LW) heterologous *E. atala*
211 opsin proteins *in vitro* (Fig. S2A). It is also successful at reconstituting and purifying
212 active LW rhodopsins, *i.e*. in *A. japonica, E. atala, Ca. sheridanii* and *Ce. ladon* lycaenid
213 butterflies (Fig. 3B-F, Fig. S2B, Table S5).

214 When purified from large-scale HEK293T cell cultures and reconstituted *in vitro* in
215 the dark in the presence of 11-*cis*-retinal, we found that the LW rhodopsin from *A.*
216 *japonica* absorbs maximally at λ_{max}= 574 ± 4 nm ($CI_{95\%}$ = 570-586 nm) (Fig. 3C) whereas
217 that of *E. atala* absorbs maximally at λ_{max}= 569 ± 2 nm ($CI_{95\%}$ = 565-573 nm) (Fig. 3D).
218 The peak of absorbance of purified LW rhodopsin measurements is within confidence
219 intervals of the best fit for LW linear absorbance estimates *in vivo* and supports the
220 hypothesis that the LW rhodopsin limb of absorbance in these two species pushes red
221 sensitivity above 600 nm. The LW rhodopsin pigment from *Ca. sheridanii* absorbs
222 maximally at λ_{max} = 519.2 nm ± 1.1 ($CI_{95\%}$ = 517-521 nm) (Fig. 3E), which is in
223 accordance with photochemical measurements (Fig. 1C), whereas *Ce. ladon* LW
224 rhodopsin absorbs maximally at λ_{max}= 531.7 ± 1.5 nm ($CI_{95\%}$ = 529-535 nm) (Fig. 3F,
225 Table S5).

226 In summary, these findings indicate that our expression system can be used
227 successfully to assess the functionality of LW rhodopsins outside of the complex eye
228 environment and demonstrate that at least some hairstreaks (Theclinae) express a new
229 functional type of far-red shifted visual opsin.

230

231 ***Blue opsin mRNA expression patterns lead to enhanced eye spectral richness***

232 Following photochemical and densitometric evidence that *E. atala* butterflies likely
233 possess four rhodopsins including contributions from two blue rhodopsins, we identified

234 two differentially expressed blue opsin-like transcripts from the eye transcriptome,
235 namely BRh1 and BRh2 (Table S6). We then examined their respective mRNA
236 expression patterns in photoreceptor cells, aided by the histological reconstruction of
237 photoreceptor organization in a typical ommatidium (Fig. 4).

238 We found that *E. atala* hairstreaks have a straight, 480-micron long rhabdom
239 composed of eight longitudinal photoreceptor cells (Fig. 4A-B (a-g)) and a ninth cell
240 close to the basement membrane (Fig. 4A-B (h)). The two most distal R1-R2
241 photoreceptor cells contribute the majority of microvillar extensions from 0 to 160
242 microns, whereas R3-R4 distal cells contribute a majority of microvilli from 140 to 300
243 microns, thereby overlapping partially with R1-R2 in the distal rhabdom tier. The
244 proximal R5-R8 cells contribute most microvilli in the last rhabdom tier up to 440
245 microns, a depth where the photoreceptor cells no longer bear any microvilli and the
246 ninth cell becomes visible (Fig. 4A-B (i)).

247 This rhabdomeric analysis provided the spatial morphological insights necessary
248 to subsequently identify photoreceptor cells expressing each opsin mRNA across
249 different eye regions. Using double fluorescent *in situ* hybridization experiments in
250 transverse and longitudinal eye sections of males and females of *E. atala*, we showed
251 that LWRh is expressed in all ommatidia in the six photoreceptor cells R3 to R8 (Fig. 5),
252 which is typical of many butterfly species (25, 29). No fluorescent signal was detected for
253 the long-wavelength opsin in R1-R2 cells (Fig. 5D-F). We next examined the cellular
254 localization of the short UV and medium blue opsin mRNAs in transverse sections in the
255 dorsal eye. Using probes targeting LWRh in combination with cRNA probes for UVRh,
256 BRh1 or BRh2 mRNAs, our data provide evidence that the latter rhodopsin mRNAs can
257 be expressed in either or both R1-R2 receptor cells forming single ommatidia (Fig 5A-F).

258 We also assessed the possibility that these opsins are co-expressed in R1 and
259 R2 cells using cRNA probes for UVRh and BRh1 (Fig. 5G), UVRh and BRh2 (Fig. 5H) or
260 BRh1 and BRh2 (Fig. 5I). We find that R1 and R2 follow a one-cell one-opsin regulation
261 pattern, with mutually exclusive expression of UVRh, BRh1 and BRh2 mRNAs (Fig. 5J).
262 Females exhibit a dorso-ventral expression gradient in which BRh2-expressing cells are
263 sparse in the dorsal eye region. In the ventral retina however, all three opsins (UVRh,
264 BRh1, BRh2) are found in addition to LWRh (R3-R8) (Fig. S3).

265 Cellular expression data therefore show that both of the duplicated blue opsin
266 mRNAs encode functional transcripts. Overall, the cellular localization of blue opsin
267 duplicates in adjacent photoreceptor cells creates multiple ways in which rhodopsins are
268 distributed within individual ommatidia, forming a local stochastic rhodopsin mosaic of at
269 least six opsin-based photoreceptor classes (UV-UV, B1-B1, B2-B2, UV-B1, UV-B2, B1-
270 B2, Fig. 5j). Additional structural features of the eye may also contribute to the diversity
271 of spectral sensitivity functions of individual photoreceptors, including the spectral
272 influence from lateral filtering granules found in distal rhabdomeres that add to the
273 spectral sensitivity of some photoreceptor cells.

274

275 ***BRh1 and Brh2 opsin duplicate loci encode blue and green-shifted rhodopsins***

276 We reconstituted active BRh1 and BRh2 rhodopsins *in vitro* and measured their
277 spectral sensitivities via spectroscopy as detailed in the methods. We determined that
278 BRh1 λ_{max} = 435 nm ± 2 nm and BRh2 λ_{max} = 500 nm ± 2 nm (Fig. 6A-B, Table S7),
279 thereby confirming that they encode the rhodopsins conferring the expanded blue to
280 green spectral sensitivity in *E. atala*. In addition to its LWRh red-shifted opsin (Fig. 3D),
281 *E. atala* uses a fourth rhodopsin that absorbs UV wavelengths *in vitro* at λ_{max}= 352 nm ±
282 3.5 nm ($CI_{95\%}$ = 345-360 nm) (Fig. 3, Fig. S2d, Table S7).

283

284 ***Four spectral tuning sites and epistasis leads to bathochromic shifts between***
285 ***blue duplicates***

286 In order to understand the proximate mechanisms driving the 65 nm spectral shift
287 between blue opsin duplicates, we performed homology modeling against the
288 invertebrate squid rhodopsin (72). Along with their 380-aa long opsin protein sequences,
289 Eat-BRh1 and Eat-BRh2 exhibit 101 amino acid residue differences (corresponding to
290 73% similarity in aa sequence). Six variant sites were identified among 21 homologous
291 residues located within 5Å of any carbon forming the *cis*-retinal binding pocket (Fig.
292 6A,C). Two variant sites (S1 and S4) are shared with a blue/violet opsin duplication that
293 occurred independently in pierid butterflies, causing a UV-shift (VRh λ_{max} = 420 nm) from

294 the ancestral blue rhodopsin (BRh λ_{max} = 450 nm) (27), whereas four residues are
295 unique to duplicated blue opsins found in lycaenids (S2, S3,S5,S6).

296 Given this combination of shared and unique yet limited number of variant sites,
297 we decided to test their possible involvement in blue spectral tuning by site-targeted
298 mutagenesis. Specifically, we first modified individual residues S1 to S4 and measured
299 their spectral tuning effect *in vitro* (Fig. 6E-G, Fig. S4). Chimeric opsins showing
300 bathochromic shifts were used sequentially to substitute adjacent variant sites following
301 two candidate evolutionary trajectories. We observed an additive bathochromic shift
302 totaling 40 nm (λ_{max} = 475 nm) by substituting A116S together with I120F and Y177F
303 (S1, S2 and S4, Fig. 6E). In a second tuning trajectory, we observed that Y177F alone
304 conferred a 79 nm bathochromic shift (λ_{max} = 514 nm), which could then be
305 compensated by a 6 nm hypsochromic shift (λ_{max} = 508 nm) by combining G175S and
306 A116S (Fig. 6G). A third evolutionary trajectory explored the contribution of two lycaenid-
307 specific cysteine substitutions (I106C, F207C) in helix 5 (Fig. S4). These changes
308 caused a strong green-wave spectral shift that was not compensated for by additional
309 candidate interacting residues in the quintuple mutant (S1,2,4,5,6; Fig. S5, Table S8).
310 G165S (S3) tested alone or in various double mutant combinations caused
311 bathochromic shifts, but we did not obtain the sextuple chimeric construct bearing
312 G175S (S3) and cannot therefore exclude the possibility that it also plays a role in this
313 case. The available results from all variants bearing cysteines in S5 and S6, however,
314 suggest that both cysteine residues on helix 5, which are absent in Pieridae blue opsins,
315 are unlikely to be the main evolutionary drivers of blue spectral shifts in lycaenid BRh2
316 loci.

317 Finally, our optophysiological density analyses showed that blue spectral
318 sensitivity differs between species equipped with green or red LW rhodopsins. Whereas
319 all species possess a blue photoreceptor with conserved absorbance with λ_{max} = 435-
320 440 nm, the second blue sensitivity peak in *A. japonica* and *E. atala* is at λ_{max} = 500 nm
321 (Fig. 2F, S5A) unlike λ_{max} = 489 in *C. ladon* (Fig. S6B, Table S9). These data suggest a
322 role for coordinated shifts between blue and LW rhodopsins in the evolution of red
323 spectral sensitivity.

324

325 ***Shifted Blue and LW rhodopsins tune colour vision in the context of conspecific***
326 ***recognition***

327 In order to investigate possible correspondence between *E. atala* visual spectral
328 sensitivities and colour traits that might be important in signalling and sexual selection,
329 we measured the reflectance spectra associated with specific wing patches (Fig. 7, SI
330 Dataset 2). For the butterfly to interpret colours, it must i) possess at least two spectral
331 types of receptors sensitive to the reflectance spectrum of incident visible light
332 illuminating the coloured area, and ii) be able to compare individual receptor responses
333 neurally to create an output chromatic signal (73). Although we did not take this analysis
334 to the second step of recording responses of different individual receptors to reflectance
335 spectra, we investigated in detail the first necessary condition by measuring and
336 comparing reflectance spectra of body and wing patches from males and females
337 including blue scales on the abdomen and thorax, as well as black, blue and red scales
338 on forewings and hindwings (Fig. 7A). In males, dorsal forewings are bright iridescent
339 blue in summer, whereas scales appear more generally green/ teal in winter generations
340 (68). Female dorsal wings, on the other hand, display a darker royal blue colour along
341 the edge of their upper forewings. Both sexes also have conserved wing and body
342 patterns, including regularly spaced rows of blue spots visible on folded and unfolded
343 hindwings, and a bright red abdomen with a large bright red spot on the mid-caudal
344 hindwing area that falls precisely along the abdomen in folded wings (Fig. 1A, inset).

345

346 First, epi-microspectrophotometry measurements from dark areas of male and
347 female wings (Fig. 7B) showed that black scales are only 1 % as reflective as adjacent
348 cyan scales in the blue/green band at 450 nm, with a reflectance maximum of 0.053
349 (female, *f*) and 0.041 (male, *m*) (SI datafile 2) compared to reflectance maxima at 510
350 nm of ventral hindwing blue scales 1.53 (*f*) and 1.76 (*m*) (Fig. 7B). This indicates that
351 brightness – which is a function of reflectance - in black regions decreases 100 fold
352 compared to adjacent coloured scales in both sexes.

353 Blue scales on the dorsal forewings have a maximal reflectance peak at 490 nm
354 in females and 510 nm in males, and blue scales on the ventral hindwings have a

355 maximal reflectance peak at 510 nm (*f*) and 530 nm (*m*) (Fig. 7B). Thorax scale
356 reflectance is 1.86 times and 2.88 times higher than dorsal wing reflectance in females
357 and males, respectively.

358 Red scales on male and female hindwings reflect maximally in the far red (750
359 nm), similarly to abdominal scales (Fig. 7B-C). Blue scales on the thorax have a maximal
360 reflectance peak at 490 nm in both sexes, overall indicating that male and female
361 reflectance spectra are similar for blue scales on the body, but not for blue scales on the
362 wings. We noted, too, that leaf surfaces of the butterfly's primary host cycad, *Zamia*
363 *integrifolia*, have a peak of reflectance at 550 nm and a red edge inflection point around
364 700 nm with high reflectance in the near infrared region (Fig. 7D). Altogether, our
365 analyses support that the butterfly's photoreceptor spectral sensitivities (Fig. 7E) can
366 efficiently discriminate between its host plant (for oviposition), the colours of male and
367 female conspecifics, and colour variation between sexes.

Discussion

Red opsin receptors contribute to far-red spectral sensitivity

It has remained challenging to identify the contribution of different genetic mechanisms that affect phenotypic variation amongst complex traits in nature, and ultimately an organism's fitness. Opsins represent a robust system to link molecular changes to phenotypic changes in animal colour vision as they are the first elements in phototransduction cascade and have been shown to directly modulate the visual spectral sensitivity of insects, primates and other vertebrates. .We have optimized a functional assay to disentangle the contribution of the long-wavelength (LW) rhodopsin from filtering pigment granules and variable eye reflectance properties in the eyes of lycaenid butterflies. We discovered a novel functional form of LW rhodopsin with a red-shifted maximal absorbance spectrum (λ_{max}) between 565 and 575 nm in two lycaenid species, *A. japonica* and *E. atala,* that is further supported by microspectrophotometry (MSP) and optophysiology data (Figs. 1-3, Fig S5). The red-shifted rhodopsins have a longer-wavelength limb of absorbance than lycaenid green LW rhodopsins due to a bathochromic shift in their λ_{max} (Figs. 1, 3), which elevates the photoreceptor response at long wavelengths (Fig. 2F, S5A). Consequently, those two species have much greater optophysiological sensitivity in the far red than the lycaenid species with photoreceptors expressing green LW rhodopsins, whether or not surrounded by lateral filtering pigments.

Red spectral sensitivity has previously been examined *in vivo* notably in a species of cabbage white butterfly, *Pieris rapae*, where light perception above 600 nm results from ommatidia expressing a single LW opsin together with two types of pigment granules that confer three types of red photoreceptors (48). Methods employing cAMP-dependent heterologous spectroscopy identified maximal peak absorptions at 540 nm and 560nm for *Papilio* PxRh1 and PxRh3 LW opsins respectively (62), whereas earlier electrophysiological λ_{max} estimates placed PxRh1 at 525 nm and PxRh3 at 575 nm (45). Our assay provides quantifiable expression and yields to obtain accurate λ_{max} *in vitro* outside of the complexity of the eye structure itself which circumvents potential inaccuracy from optophysiological estimates measured *in vivo* in certain species due to interfering lateral pigments or other properties of the eye itself. It also has the advantage

400 of functionally studying variation in orthologous rhodopsin genes independently from
401 inferences based on sequence data alone. Our study reconciles *in vivo* and *in vitro*
402 approaches to substantiate that higher visual performance in the far red is achieved by
403 modifying absorbance properties of long-wavelength rhodopsins.

404

405 ***Duplication, spectral tuning and adjacent cellular localization provide expanded***
406 ***photoreceptor types***

407 Opsin evolution has undergone recurrent events of gene duplication and loss across
408 animals including insects (16). From ancestral insect trichromatic colour vision (UV, blue,
409 green), insects that have lost one of these three rhodopsins are often found to have
410 compensated from that loss by recruiting a duplicate gene copy that has undergone
411 spectral tuning to shift the peak sensitivity, as seen in true bugs and beetles (23, 39). By
412 contrast, tetrachromatic insects that activate an additional rhodopsin are also known to
413 have acquired increased spectral sensitivity in ranges of visible light, as seen in
414 *Heliconius* duplicated UV opsins (21), or *Pieris* duplicated blue opsins (27). Lycaenid
415 species examined thus far have two blue opsins for which epi-microspectrophotometric
416 estimates previously yielded sensitivities of λ_{max} in the range 420-440 nm and 480-500
417 nm (40, 41).

418 Our results show that blue opsin loci in *E. atala* specify blue and green-shifted
419 rhodopsins (Figs 2,6) similarly to species of *Lycaena* and *Polyommatus* (40, 41). The
420 most striking functional insight in the evolution of blue spectral tuning in *E. atala* comes
421 from chimeric BRh1 variants bearing mutations A116S, G175S and Y177F, which confer
422 a 73-nm bathochromic shift (λ_{max} = 508 nm) that most closely recapitulates the spectral
423 properties of Eat-BRh2 (λ_{max} = 500 nm) compared to other tested variants (Fig. 5G, Fig
424 S4). Intermediate adaptive phenotypes can also be revealed via gradual evolutionary
425 trajectories. Eat-BRh1 variant A116S causes a +5 nm shift alone, but together with
426 I120F, shifts maximal absorbance by an additional +15 nm to λ_{max} = 455 nm. Since these
427 two residue substitutions are conserved across all characterized lycaenid BRh1 loci (Fig.
428 3A), these results show how adjacent sites in helix 3 can contribute to intermediate blue
429 absorbance spectra across lycaenids.

430 The third tuning residue, Tyr177Phe is a key spectral tuning mutation in *E. atala,*
431 since the triple BRh1 variant (A116S/I120F/Y177F) displays a 30 nm bathochromic shift
432 (λ_{max} = 475 nm) compared to its native rhodopsin, and illustrates the multiple ways that
433 gradual spectral tuning can evolve, at least in this species. Two of the reverse tuning
434 substitutions are the same sites responsible for hypsochromic spectral shifts both in a
435 blue-shifted LW rhodopsin of a *Limenitis* butterfly (Y177F, -5 nm) (61) and in a violet-
436 shifted blue rhodopsin of a *Pieris* butterfly (S116A, -13 nm; F177Y -4 nm) (27), stressing
437 the importance of tuning residues lying on the ionone ring portion of the chromophore
438 binding pocket. Spectral tuning modulation in blue-rhodopsin duplicate functions has
439 therefore involved conserved biochemical constraints along independent evolutionary
440 trajectories that selected for partial spectral tuning sites in rhodopsin G-coupled
441 receptors. Reverse mutations are not functionally equivalent in their absolute
442 magnitudes ($\Delta\lambda_{max}$), therefore underscoring the role of epistatic interactions with
443 neighbouring sites resulting in distinct λ_{max} shifts across butterfly lineages.

444 Molecular and phylogenetic studies of opsin evolution in vertebrates have also
445 shown that homologous tyrosine residues in the ionone ring portion of the chromophore-
446 binding pocket (e.g. Y262) in the human blue cone opsin (λ_{max} = 414 nm) are responsible
447 for a 10 nm bathochromic spectral tuning when mutated to Tryptophan (Trp) (74). This
448 illustrates that distant opsin loci meet similar structural and biochemical constraints as
449 those observed in the evolution of vision genes in other vertebrates (11, 14). However,
450 Y177 is unique to *E. atala*, and other BRh1 loci at this position readily possess the F177
451 similarly to Eat-BRh2 (Fig. 3A). Not all BRh2 loci have S175 but instead keep G175 in
452 both blue loci, suggesting an additional yet unknown role for adjacent residues in
453 positions R176K and I178V. The latter residues do not differ highly in hydrophobicity but
454 may still provide the necessary molecular interactions with the ionine ring portion of the
455 chromophore necessary to modulate variable BRh2 spectral phenotypes. Human
456 ancestors also achieved blue sensitivity gradually and almost exclusively via epistasis at
457 seven amino acid residues (55). By studying independent opsin gene duplicates in the
458 butterfly family Lycaenidae, our *in vitro* assays refine our understanding of the molecular
459 basis of convergent colour vision phenotypes and help to identify key determinants of
460 genotype-phenotype relationships across insect blue opsins, although these are only a
461 snapshot of all possible chimeric blue rhodopsin variants along at least three possible

evolutionary trajectories. Testing the non-additive interactions at co-evolving BRh2 adjacent sites (175-178) in lycaenids lacking red sensitivity will help to fully recapitulate intermediate phenotypes across derived blue-shifted rhodopsin duplicates in addition to those generated by A116S and I120F.

In theory, a typical tetrachromat can achieve better wavelength discrimination than a typical trichromat (55, 73) because of the interplay between additional gene copies and the coevolution of spectral tuning across rhodopsins decreases the minimal wavelength difference (Δλ) that an insect can discriminate. *Papilio* butterflies, for instance, have some of the most complex retinal mosaics known, with three ommatidial types expressing various combinations of five rhodopsin proteins (UV, B, 3 LW), as well as filtering pigments that produce diverse ommatidial spectral sensitivities (29, 45). Amino acid residues in helix 3 have been shown to mediate an absorbance shift between duplicates LW PxRh1 and PxRh3 in *Papilio (62)*, but lycaenid LW opsins possess a highly conserved helix 3 that does not exhibit any of the spectral substitutions found across Papilionidae, supporting the hypothesis that distinct spectral tuning mechanisms have evolved independently in invertebrate LW opsins. Future work will be able to disentangle the spectral tuning mechanisms of LW opsins *in vitro* using the recombinant purification system described here.

In *E. atala*, ommatidial density and expression profiling showed that photoreceptor cells containing BRh2 are less abundant (~25%) compared to those containing UV (~50%) and BRh1 (75%) rhodopsins. In spite of its low density across the eye, the derived green-shifted blue rhodopsin improves signal resolution in the green spectrum and provides direct adaptive benefits for light perception in both males and females. Compared to trichromats, the expanded six-ommatidial types primarily derive from the non-overlapping cellular expression of BRh1 and BRh2 rhodopsin mRNAs in distal rhabdomeric cells. Together, the stochastic rhodopsin mosaic offers remarkable properties that could not be achieved with the limited sensitivity of a single blue opsin gene.

491 In summary, our results support the scenario of a sensory system in which gene
492 duplication generates new opsin paralogs, cis-regulatory changes generate new
493 photoreceptor subtypes via gene-specific expression patterns, and coding mutations
494 tune the spectral sensitivity maxima of two of the four rhodopsins (BRh2, LWRh). All of
495 these changes have contributed to the diversification of visual spectral sensitivities,
496 thereby enhancing colour discrimination.

497

498 ***Co-evolving shifts at blue and red opsins tune intraspecific visual signalling***

499 Additional structural features of the eye can contribute to spectral sensitivity of
500 individual photoreceptors at long wavelengths, including lateral filtering granules found in
501 distal rhabdomeres. However, here the primary mechanism pushing red sensitivity is
502 through functional divergence at the LW rhodopsin locus. This remarkable novelty
503 provides a two-factor interaction (Blue-LW) to modulate green-red sensitivity among
504 closely related taxa.

505 Building on earlier butterfly microspectrophotometry work (19, 40, 41, 53), our
506 study shows that lycaenid species with red-shifted LW opsins have their second
507 maximum sensitivity peak and associated blue rhodopsin shifted to green maximal
508 absorbance with λ_{max} 495-500 nm. By contrast species with a LW ancestral-green opsin
509 with λ_{max} 520-530 nm have their second maximum sensitivity peak at blue wavelengths
510 λ_{max} = 480-490 nm (Fig. 1C, S6A), suggesting modulatory benefits for coevolving
511 spectral shifts at multiple rhodopsins. Within Lycaenidae, reflectance patterns of wing
512 scales have been investigated in the genera *Celastrina* and *Callophrys* (75, 76) and
513 these studies support a scenario of co-evolution of spectral shifts across opsins. The
514 ventral wings visible at rest in Green Hairstreak lycaenids (genus *Callophrys*) typically
515 appear green and consist of yellow and bluish scales with an omnidirectional reflectance
516 peak in the green slightly above 550 nm (76). *Celastrina* species tend to display bright
517 blue coloured wings, which predominantly reflect light in the UV-blue band (75) and can
518 thus be perceived by comparing neuronally the spectral input from light activating retinal
519 photoreceptors expressing both UV/ blue rhodopsins without requiring expanded red
520 sensitivity.

521 These observations suggest a role for molecular tuning of blue and LW opsin
522 genes in driving the dynamic evolution of green-red spectral sensitivity. Extant human
523 trichromatic colour vision is similarly thought to have evolved via spectral tuning of
524 existing short wavelength-sensitive opsins in concert with molecular variation at
525 duplicated opsin loci leading to middle and long-wavelength sensitivities (55). Ultimately,
526 mechanistic and functional studies of spectral tuning evolution in different orthologs in
527 additional species will enable us to infer the ancestral states and better resolve the
528 evolutionary time scale involved in stages of spectral tuning of blue and red sensitivities
529 across lycaenids.

530

531 ***Colour tuning improves intraspecific signal detection***

532 Two effects of molecular variation in visual pigments in *E. atala* are that its eyes have
533 expanded spectral sensitivity at longer wavelengths as well as increased spectral
534 discrimination in the blue band. In order to investigate the evolutionary consequences of
535 molecular changes in butterfly opsins in the broader context of behaviours requiring
536 colour vision, such as finding oviposition sites, and intraspecific recognition (37, 77-80),
537 we need to analyze the degree of overlap of spectral sensitivities (73) and evaluate this
538 against the spectral composition of the reflected light of the background and other
539 objects, such as that produced by foliage and conspecifics.

540 The limiting wavelength at which only the human L cone opsin (λ_{max} = 559-563
541 nm) is sensitive corresponds to approximately 625 nm (81), which is the wavelength at
542 which orange-red can be discriminated from pure red in human colour perception. The
543 human neighboring M cone rhodopsin is at λ_{max} = 530 nm, which at 625 nm, has a
544 sensitivity of 0.05 (81). By extension, for *E. atala*, BRh2 has a sensitivity of 0.05 at 613
545 nm (Fig. 2, Fig. 6), indicating that R565 would perceive 'pure red' wavelengths of light
546 from 613 nm onwards. Alternatively, we can compute the relative sensitivity of the LW
547 rhodopsin at 700nm (3%, Fig. 1, Fig. 3), which is generally accepted as the limit for
548 photopic vision, and then identify the corresponding wavelength at which BRh2 reaches
549 that same sensitivity, which is 619 nm (Fig. 2). Conservatively, we can conclude that the
550 red rhodopsin together with the green-shifted blue rhodopsin BRh2 of *E. atala* contribute

551 to the perception of colours at long-wavelengths up to 613 nm. The LW rhodopsin
552 sensitivity in *A. japonica* is similar to *E. atala*, and the green-red visual spectral
553 sensitivities of *Arhopala* butterflies would capture the dorsal wing secondary reflectance
554 peak between 500-600 nm, which is absent in *Celastrina* or *Callophrys* wings (75).
555 Dorsal *Arhopala* wings also have velvety black edges filled with blue regions that
556 primarily reflect light at 370 nm in males and 400 nm in females (82) and further benefit
557 from the expanded blue sensitivity seen across lycaenid butterflies. Similarly to super-
558 black plumage colouration in birds (83), peacock spiders (84), and recent examples in
559 papilionids and nymphalid butterflies (85), the adjacency and sex-specific regions
560 covered with structural velvety black scales in the lycaenid *E. atala* likely enhance the
561 perceived brightness of nearby colour signals.

562 Our wing scale analysis indicates that red colour discrimination is important to
563 see conspecifics due to their striking reflectance above 600 nm (Fig. 7A). Reflectance
564 spectra from the red abdomen and the ventral hindwing are similar and overlap spectral
565 sensitivities of two rhodopsins (LWRh and BRh2), meaning the butterfly can not only
566 detect brightness but can also derive a colour signal from these patterns, and separate
567 these input signals from those of environmental colour cues such as signals produced by
568 foliage (Fig. 7D) (86). Abdominal reflectance in the range 613-619 nm is roughly a third
569 of its maximal reflectance, but there is substantial overlap of the abdomen's spectrum
570 with BRh2 spectral sensitivity, which suggests that the Atala hairstreak's colour
571 perception of the abdominal colour of conspecifics is not pure red, but something more
572 like Orange-Red. All *Eumaeus* species have this orange-red colouration and the red
573 scale reflectance spectra are similar between the sexes, suggesting that it evolved at the
574 base of the *Eumaeus* genera, as an aposematic signal driven by the association with
575 cycads. Whereas our results show a clear sex-specific reflectance difference on dorsal
576 wings, it is unclear whether the red warning colouration patterns may have been coopted
577 as a conspecific signal, as in other unpalatable butterflies (79, 87) , in which case it could
578 be a by-product of the evolution of a signal used primarily to avoid predation. Hence, the
579 L cones of most birds have red sensitivity from about 550 nm to 700 nm (59, 88), and
580 the bright red abdominal/ hindwing reflectance in the near-infrared spectrum would
581 stimulate mostly bird LWS /red (without MWS/ green) to perceive a colour close to "pure
582 red".

583 Lycaenid butterflies with four rhodopsins can see more colour hues in the blue-
584 green range than mammals that have either di or trichromatic vision (34). Sex-specific
585 scale reflectance spectra on dorsal wings convey colour information that is readily
586 distinguishable by the visual system. Our study, by showing the expanded spectral
587 sensitivity exhibited by lycaenid butterflies through molecular variation and functional
588 changes in their 4-rhodopsin visual system, highlights the importance of peripheral
589 sensory genes in driving the adaptive evolution of multi-modal communication.

590 ## Materials and Methods

591
592 *Butterflies*

593 Pupae of *Eumaeus atala* were collected from host plants of *Zamia integrifolia* (locally
594 known as "coontie") at the Montgomery Botanical Garden, Miami, FL, USA and reared at
595 22°C in an insectary in the MCZ laboratories under a 12:12 L:D cycle until emergence.
596 *Callophrys sheridanii* and *Celastrina ladon* were collected on Badger Mountain,
597 Wenatchee WA, USA and Wahclella Falls, OR, USA respectively. Eggs and young
598 larvae of *Arhopala narathura japonica* were collected feeding on oak trees (*Quercus*
599 *glauca*) from field sites near Ginoza, Okinawa, Japan and reared in the laboratory in
600 Cambridge, MA, USA until they eclosed as adults.

601

602 *Epi-Microspectrophotometry*

603 Quantitative epi-microspectrophotometry (epi-MSP) was used to determine absorption
604 spectra of butterfly rhodopsins by measuring eyeshine reflectance spectra after
605 photoconversion of the rhodopsin to its metarhodopsin product (54, 89).
606 Compound eyes of most adult butterfly species exhibit eyeshine, a property that
607 allows measuring rhodopsin absorbance spectra as well as spectral sensitivity of
608 photoreceptor pupillary responses in eyes of intact butterflies. When subjected to
609 repeated bright white flashes under incident-light microscope, 1) there is a
610 photochemical effect, i.e. the coloration of eyeshine changes during each flash owing to
611 changes in absorbance spectra that accompany photo-isomerization of rhodopsins to
612 their metarhodopsin photoproducts (89); and 2) there is a pupillary response mediated
613 by intracellular migration of pigment granules within photoreceptor cells, causing the
614 intensity of eyeshine to decrease rapidly with time during each flash (90).
615 Three MSP methods (*in vivo* Photochemistry, Optophysiology, Retinal
616 densitometry) are critical to study rhodopsin properties. The methods are presented
617 here, whereas the rationale upon which the three methods are based and the general
618 procedures for using eyeshine to make photochemical measurements from butterfly
619 eyes are described in detail in SI methods.

620

621 *In vivo* Photochemistry

622 When rhodopsin is photo-isomerized to become metarhodopsin, it undergoes a spectral
623 shift in the absorbance spectrum. For LW rhodopsins, the shift is to shorter wavelengths;
624 the metarhodopsin peak is usually between 490 nm and 500 nm. For both UV-absorbing
625 and blue-absorbing rhodopsins, the shift is to longer wavelengths, typically to 475 nm -
626 490 nm. These photochemical changes are observable in eyeshine reflectance spectra,
627 as increased reflectance caused by loss of rhodopsin, and decreased reflectance
628 caused by the metarhodopsin. The computed absorbance-difference spectrum (DS),
629 therefore, has a positive peak caused by accumulation of metarhodopsin (M), and a
630 negative peak caused by loss of rhodopsin (R) (Fig. 1, 2A).

631 The absorbance difference spectrum relaxes with time in the dark, but changes
632 shape in doing so; the positive peak relaxes to zero much faster than the negative peak.
633 The entire temporal evolution of difference spectra can be reproduced quantitatively by
634 assuming different kinetics for the dark-processes of metarhodopsin decay and
635 rhodopsin recovery. Metarhodopsin decay is well approximated by a single exponential
636 process, but the time constant is a strong function of temperature. Rhodopsin recovery
637 is considerably slower than metarhodopsin decay, making it possible to create a partial
638 bleach using repeated episodes of bright flashes followed by dark periods during which
639 metarhodopsin decays totally from the rhabdom. The difference spectrum for that partial
640 bleach is a direct measurement of the absorbance spectrum of the LW rhodopsin (Fig. 1)
641 (89). Similar experiments with photoconversion of the other spectral types of rhodopsin
642 are more complicated because a bright blue flash designed to efficiently photo-isomerize
643 blue-absorbing rhodopsin will also convert some LW rhodopsins to their
644 metarhodopsins, although with less efficiency. However if the LW rhodopsins are first
645 bleached, then difference spectra for the blue rhodopsin are measurable (Fig. 2A).

646 Photochemical measurements of the *E. atala* blue rhodopsin were done with a
647 male oriented similarly to the female at Elevation 0° and Azimuth 10°. Before
648 photoconversion of the blue rhodopsin, the LW rhodopsins were partially bleached by
649 flashing with 20s exposure to RG645 (20s, 2s/55s). After resting in the dark for 24 min
650 for metarhodopsins to decay, the eye was flashed with 12s RG430 (2s/60s), which

651 converted blue rhodopsin to its metarhodopsin M505. A difference spectrum for R440
652 was computed from reflectance spectra measured before and 9 min after the series of
653 bright blue flashes.

654

655 *Optophysiology*

656 Photoreceptor cells in butterfly eyes contain intracellular pigment granules that move
657 centripetally in response to bright illumination and deplete light from the rhabdom by
658 scattering and absorption. This process creates an effective pupillary response
659 observable as a decrease in eyeshine reflectance (90). This intracellular pigment
660 migration is mediated exclusively by photo-isomerization of the rhodopsin contained
661 within the same cell's rhabdomere and is not influenced by physiological responses of
662 neighboring ommatidia. Thus, the pupillary pigment granules can be used as an optically
663 measured intracellular probe of physiological responses to light from that cell (91).
664 A double-beam Epi-MSP apparatus was used for optophysiological
665 measurements of eyeshine. One beam is deep-red filtered (e.g., 710 nm), that monitors
666 continuously the reflectance of eyeshine but does not itself cause a pupillary response.
667 The second beam delivers a monochromatic flash that evokes a pupillary response,
668 measured by the first beam as a decrease in deep-red eyeshine reflectance. At each
669 stimulating wavelength, the flash intensity is adjusted with computer-controlled neutral-
670 density wheels to produce a criterion decrease in reflectance (usually 3% - 5%).
671 Wavelength sequence is randomized. Both flash duration and inter-stimulus interval are
672 held constant. After completing an experimental series, the butterfly is replaced by a
673 factory calibrated Hamamatsu S1226 photodiode and quantum flux Q measured for
674 every criterion combination of wavelength and wheel setting. Spectral sensitivity is
675 computed as $S(\lambda) = 1 / Q(\lambda)$.

676

677 *Retinal Densitometry*

678 The visual pigment content of rhabdoms can be estimated quantitatively when the
679 tapetal reflectance spectrum is constant (white) for wavelengths shorter than about 600
680 nm (25, 92). A computational model based on an electron micrograph of the tracheolar

681 tapetum shows that this "chirped" set of layers functions as a broadband reflecting
682 interference filter exhibiting a computed reflectance greater than 90% for wavelengths
683 between 320 and 680 nm, thereby justifying the assumption of a white reflectance
684 spectrum in that band. This property of wideband white tapetal reflectance can be
685 exploited to computationally estimate rhodopsin contents. It is most valuable when
686 applied after λ_{max} of UV, blue, and LW rhodopsins have been determined from *in vivo*
687 photochemistry (Fig. 1; Fig. 2A) and optophysiology (Fig. 2B). R360, R440, and R565
688 have been determined in *E. atala* (Fig. 2C-D).

689 The procedure is sequential. First, a reflectance spectrum was measured after all
690 metarhodopsins had decayed from the rhabdoms, e.g., after overnight dark-adaptation
691 (black filled circles). Next, the dark spectrum was stripped of round-trip optical density
692 (OD) 1.50 (*male, m)* or 1.00 (fe*male, f*) of R565 rhodopsin so that the residual spectra
693 (red lines) were flat from 570 nm out to the 690 nm roll-off of tapetal reflectance. Next,
694 those residual spectra were stripped of OD 0.36 (*m*) and 0.22 (*f*) of R440 (cyan lines),
695 leaving large dips in the blue-green around 500 nm that were poorly fit by a single blue
696 opsin. However, stripping of OD 0.72 (*m)* and 0.55 (*f)* λ_{max} 395 (Retinal Binding Protein,
697 RBP) left UV residues (magenta lines) well fit by density of 0.55 (*m*) and 0.55 (*f*) of R360.
698 The remaining residuals (blue lines) were subjected to least-squares fitting to the
699 rhodopsin template (Fig. 2E), which produced excellent R495 fits of 0.39 (*f*) and 0.70
700 (*m*), supporting the presence of the fourth rhodopsin, R495.

701 The spectral sensitivities of *Arholopa, Celastrina and Callophrys* rhodopsins were
702 investigated using the same techniques as described in SI methods.

703

704 *De novo* E. atala *eye transcriptome*

705 The heads of 10 adult males (1 day old) were dissected under ambient light with their
706 antennae and palpi removed prior to flash freezing in liquid nitrogen. Total RNA was
707 extracted using the Direct-zol RNA extraction kit (Zymoresearch, CA, USA). Illumina
708 paired-end libraries were constructed using the Ultra II RNA Directional kit (New England
709 Biolabs, USA) and sequenced with an Illumina HiSeq v4. Adaptors were removed using
710 Trimgalore (93) and low quality reads were filtered out prior to generating a *de novo*

711 assembly reference transcriptome for all libraries in the Trinity sequence assembly and
712 analysis pipeline (94). This assembly resulted in 301656 transcripts with a contig N50 of
713 2519 bp, and average contig lengths of 1029 bp. Small fragments were filtered out
714 based on expression values using Kallisto(95). Opsin sequences from two other
715 lycaenids (41) were used as queries to identify all opsin mRNAs across tissues in the
716 final assembly using BLAST(96). To confirm their identity, the candidate opsin
717 sequences were blasted back to the NCBI non-redundant database.

718 *Lycaenid Blue and LW opsin cDNA characterization*

719 RNA was extracted from eye tissue preserved in RNA shield reagent (Zymo Research)
720 for *A. japonica, Ce. ladon and Ca. sheridanii*. Samples were first removed from the
721 storage solution with sterile forceps, briefly blot dried on a sterile Kimwipes paper, flash
722 frozen in a mortar containing liquid nitrogen and finely ground using a cold pestle.
723 Following RNA purification, we quantified RNA using a Quant-iT RNA kit and a Qubit
724 fluorometer (Invitrogen). From purified RNA, we synthesized cDNA using the The
725 GoScript™ Reverse Transcription System (Promega) and amplified a central region of
726 the long-wavelength opsin using degenerated oligonucleotide primers 5'-
727 TTGAAGCTTCARTTYCCNCCNATGAAYCC-3' (forward) and 5'-CGAATTCGTCAT
728 RTTNCCYTCIGGNACRTA-3' (reverse) (48). Single bands of expected sizes were
729 obtained, and the PCR products were purified with Exo-SAP, following Sanger
730 sequencing. We thereafter used the SMARTer RACE cDNA Amplification kit (Clontech)
731 to prepare 5'- and 3'- RACE cDNA for each species. We carried out RACE PCRs, and to
732 increase the specificity of RACE reactions, we performed nested PCRs for each cDNA
733 and obtained single-band PCR products, which were gel-purified using a Qiaquick Gel
734 Extraction Kit (Qiagen), ligated into PCR2.1 Vector kit (Invitrogen) and transformed into
735 competent TOPO10 cells (Invitrogen). Single bacterial clones were purified, and plasmid
736 DNAs were sequenced using M13F and M13R primers at the Harvard DF/HCC DNA
737 Resource Core. In total we obtained sequences from 5 to 10 opsin clones for each
738 RACE cDNA. Based on the 5'- and 3'-UTR information, gene-specific primers were
739 designed and used in combination with respective eye cDNAs to confirm the integrity of
740 each full-length LW opsin coding frame sequence. Opsin subfamily phylogenetic
741 placements were confirmed by aligning selected lepidopteran opsin genes extracted

742 from Genbank using the MAFFT package as implemented in Geneious(97), and a
743 Neighbor-Joining (NJ) tree of the aligned dataset was constructed using RAxML(98).

744

745 *Cloning and protein expression*

746 The coding region of each opsin transcript was amplified from eye cDNA and subcloned
747 in a modified pFRT-TO expression vector cassette derived from pcDNA5 and containing
748 the human cytomegalovirus (CMV) immediate early promoter (Invitrogen, USA). The
749 expression plasmid was modified to include a C-terminal tag by the monoclonal antibody
750 FLAG epitope sequence (DYKDDDDK), followed by a Ser-Gly-Ser linker peptide, a T2A
751 peptide sequence (EGRGSLLTCGDVEENPG) and the fluorescent marker protein
752 mRuby2. Plasmid DNAs were verified by Sanger sequencing and purified with the endo-
753 free ZymoPURE™ II Plasmid Midiprep Kit (Zymo Research, USA). Two micrograms of
754 plasmid DNAs were used to transfect small-scale HEKT293 cultures and optimize
755 expression conditions both via mRuby2 visualization and western blot analysis. Cells
756 were plated at a density of $0.6x10^6$ cells in a 6-well culture dish containing DMEM
757 medium (Gibco), and transient transfection was achieved after 48h when reaching 80%
758 confluency in a 1:3 ratio DNA (µg): PEI (µL) (Polysciences, USA) at 1mg/mL in
759 molecular grade water, filter-sterilized at 0.22 µm. The transfected cells were harvested
760 in cold D-PBS (Sigma-Aldrich) after 2 days, centrifuged at 4°C for 5 min at 4000 rpm,
761 and resuspended in 50 µL Ripa lysis buffer (Invitrogen) supplemented with 1% n-
762 Dodecyl β-D-maltoside (Sigma-Aldrich). Cell membranes were lysed for 1h at 4°C with
763 gentle rotation on a sample homogenizer, and cell debris collected by centrifugation at
764 4°C for 15 min at 13,000 rpm. The crude protein lysate concentration was quantified by
765 BSA (Sigma-Aldrich) and 25 µg crude extract was loaded on NuPAGE™ 3-8% Tris-
766 Acetate gels (ThermoFisher) and transferred to a polyvinylidene difluoride membrane on
767 a TurboBlotTransfer system (Biorad Laboratories). The membranes were blocked with
768 1% milk (Biorad) in phosphate-buffered saline containing 0.1% Tween 20 (PBS-T,
769 Biorad) and incubated overnight with primary antibodies (aFLAG 1:2,500, aHSP90
770 1:50,000, GE Healthcare) containing 0.01% Sodium azide (Sigma Aldrich) on a gently
771 rocking platform at 4°C. After washing with TPBS the membranes incubated with aFLAG
772 and aHSP90 were respectively incubated with HRP Conjugated ECL anti-mouse and

773 ECL anti-rabbit (Amersham, USA), revealed using the SuperSignal West Femto (Thermo
774 Scientific) and imaged on a ChemiDoc system (Biorad Laboratories).

775

776 *Transient expression, purification of expressed rhodopsins and spectroscopy*

777 High-expressing clones from GPCR opsin cDNAs were transiently expressed in
778 HEKT293 cells prior to *in vitro* purification. For each construct, cells were seeded at a
779 density of $1.0x10^6$ cells on day 0 in fifteen tissue culture dishes (10 cm diameter, ref
780 25382-166, VWR) in DMEM High Glucose, GlutaMAX (Life Technologies) supplemented
781 with 10% FBS (Seradigm Premium, VWR, USA). Lipid complexes containing 24 µg
782 DNA: 72 µL PEI (1mg/mL) diluted in Opti-MEM I Reduced Serum (Life Technologies)
783 were added 48h later to cells reaching 75-85% confluency. Six-hours post-transfection,
784 the culture medium was exchanged with new medium containing 5 $\mu.mol^{-1}$ 11-*cis*-retinal
785 (2mg/mL stock in 95% Ethanol) and under dim red illumination. The *cis*-retinal
786 absorption peak at 380 nm was confirmed using a NanoDrop™ 2000/2000c UV-VIS
787 Spectrophotometer (Thermo Fisher) prior to each experiment using a 1:100 dilution in
788 ethanol. Culture plates supplemented with cis-retinal were wrapped in aluminium foil and
789 cells were incubated in the dark. Forty-eight hours post-transfection, the medium was
790 decanted under dim red light illumination. Cells were scraped from the plates in cold
791 filter-sterilized HEPES wash buffer (3mM $MgCl_2$, 140mM NaCl, 50mM HEPES pH6.6-8.5
792 depending on protein isoelectric point) containing complete EDTA-free protein inhibitors
793 (Sigma-Aldrich), centrifuged for 10 min at 1,620 rcf at 4°C, and resuspended in 10 mL
794 wash buffer for two consecutive washes. After the second wash, cell pellets were gently
795 resuspended in 10mL cold wash buffer containing 40 µM 11-*cis*-retinal. Cells expressing
796 opsin-membrane proteins were incubated in the dark during 1h at 4°C on a nutating
797 mixer (VWR) to increase active rhodopsin complexes, and cells were then collected by
798 centrifugation at 21,500 rpm for 25 min at 4°C on a Sorvall WX Ultra 80 Series equipped
799 with an AH-629 Swinging Bucket Rotor (Thermo Scientific).

800 Transmembrane proteins were gently extracted by pipetting in 10 mL ice-cold extraction
801 buffer (3mM $MgCl_2$, 140mM NaCl, 50mM HEPES, 20% Glycerol v/v, 1% n-dodecyl β-D-
802 maltoside, complete EDTA-free protein inhibitors) and incubated for 1h at 4°C prior to

803 centrifugation at 21,500 rpm for 25 min at 4°C. The 10mL crude extract supernatant
804 containing solubilized rhodopsin complexes was added to 1mL Pierce™ Anti-
805 DYKDDDDK Affinity Resin (Thermo Scientific, USA) and incubated overnight at 4°C in a
806 15mL falcon on a nutating mixer. Samples were loaded on Pierce™ Centrifuge Columns
807 (ref 89897, Thermo Scientific, USA) and after 3 washes of the resin-bound FLAG-
808 epitope rhodopsin complexes with 3-column reservoir volumes of elution buffer (3mM
809 $MgCl_2$, 140mM NaCl, 50mM HEPES, 20% Glycerol v/v, 0.1% n-dodecyl β-D-maltoside),
810 the rhodopsin was eluted in 2mL elution buffer containing 1.25 mg (265 μM) Pierce™ 3x
811 DYKDDDDK Peptide (Thermo Scientific, USA). The eluate was concentrated using an
812 Amicon Ultra-2 Centrifugal Filter Unit with Ultracel-10 membrane (Millipore, USA), for 35
813 min at 4°C and 3,500rpm. The concentrated eluate (~350μL) was aliquoted in Amber
814 light-sensitive tubes (VWR, USA) and kept on ice in the dark. Ultraviolet-visible
815 absorption spectra (200-800nm) of dark-adapted purified proteins were measured in the
816 dark from 1.5 uL aliquots using a NanoDrop™ 2000/2000c UV-VIS spectrophotometer
817 (Thermo Fisher). Opsin purification yields were estimated following BSA analysis (Table
818 S23, SI methods). Spectroscopic analysis was performed from the mean value of 4-6
819 independent spectral measurements. Raw absorbance data were fitted to a visual
820 template (99) and polynomial functions analyses performed in R (V.0.99.486) (100)to
821 determine the opsin maximal absorption peaks.

822

823 *Preparation of RNA probes and RNA* in situ *hybridization*

824 We created *in vitro* transcription templates from UVRh, BRh1, BRh2, LWRh opsin
825 complementary DNA cloned in approximately 700-base-pair (bp) segments to pCRII-
826 TOPO (Invitrogen). Antisense cRNA probes were synthesized using T7 or Sp6
827 polymerases using either digoxigenin (DIG) or fluorescein (FITC) labelling mix (Sigma-
828 Aldrich) from gel-purified PCR templates. The synthesized cRNA probes were ethanol-
829 precipitated with NH_4OAc 7.5M and 1 μL glycogen, spun down at 4°C for 30 min, re-
830 dissolved in pure water and stored at -80°C. These RNA probes were first used to test
831 mRNA expression for each opsin receptor gene. We then tested the probes by dual
832 colour *in situ* hybridization using combinations of DIG and FITC probes to map opsin
833 receptor expression patterns.

834 For *in situ* hybridization, *E. atala* compound eyes were dissected and immersed in 1.5mL
835 eppendorf tubes containing freshly-made 4% formaldehyde (FisherScientific)/1x PBS for
836 2h at room temperature for fixation, then immersed successively in increasing sucrose
837 gradient solutions (10%, 20%, 30% in PBS) for 1h each, stored in 30% sucrose solution
838 overnight at 4°C, briefly transferred in OCT:sucrose 1:1, embedded in OCT (Tissue-Tek)
839 and frozen in dry ice. Tangential and longitudinal eye sections (12 µm) were obtained
840 using a cryostat (Leica), mounted on VWR Superfrost Plus Micro slides and used for
841 RNA *in situ* hybridization following a procedure described in details previously (101).
842 Double fluorescence *in situ* hybridization was performed using 100 µl hybridization
843 solution (pre-hybridization buffer supplemented with 4% Dextran sulfate (Sigma)
844 containing a combination of two opsin cRNA probes, one labeled with DIG and one
845 labeled with FITC (at 1ng.µl^{-1} for UVRh and BRh2, and 0.5ng.µl^{-1} for BRh1 and LWRh).

846 *Eye anatomy*

847 Each *E. atala* eye was immersed for prefixation in 2.5% Glutaraldehyde/2%
848 paraformaldehyde in 0.1M Sodium Cacodylate buffer (pH 7.4) (Electron Microscopy
849 Sciences, PA, USA) for 2h at room temperature, then stored at 4°C for 12-14h prior to
850 fixation, embedding, ultrathin sectioning and mounting on copper grids for TEM analysis
851 as described in SI methods.

852

853 *Homology modeling and targeted mutagenesis*

854 To investigate the molecular basis of spectral tuning differences between the duplicated
855 blue visual opsins, we carried out site-directed mutagenesis of amino acid substitutions
856 that could contribute to possible changes in the maximal absorption spectra of dark-
857 adapted rhodopsins. First, the Eat-B1 (λ_{max} = 435nm) and Eat-B2 (λ_{max} = 500nm) opsin
858 amino acid sequences were uploaded to the SWISS-MODEL protein recognition engine
859 (102) to generate templates aligned against the invertebrate squid rhodopsin crystal
860 structure (PDB2Z73) (72). The predicted homology model for each blue opsin was
861 analyzed in Pymol (103) to identify homologous binding sites in the *cis*-retinal binding
862 pocket within a range of 5Å from any carbon in the retinal polyene chain. Of the 101
863 amino acid substitutions that differ between the duplicate opsins, 21 residues were

predicted to interact with the *cis*-retinal chromophore, with 6 variant sites between both opsin sequences.

Amino acid sequences from blue opsins were retrieved from Genbank and aligned using the MAFFT package followed by NJ tree inference and support analysis derived from 1,500 bootstrap replicates in Geneious (97) prior to visualization in EvolView (98) with squid rhodopsin as the outgroup. The phylogeny was used to identify functionally convergent amino acid replacements repeatedly associated with similar shifts in absorption spectra between blue opsin duplicates. We identified amino acid positions that were likely to reside within the chromophore binding pocket of the opsin protein, and that also had diverging biochemical properties (charge and/or polarity).. A BRh1 plasmid DNA construct was modified to incorporate variant positions found in BRh2, namely A116S (S1), I120F (S2), G175S (S3), Y177F (S4), I206C (S5), and F207C (S6).

Chimeric BRh1 rhodopsin constructs bearing single variant sites located on helix 3 (S1, S2) and the β-strand located between helices 3 and 4 (S3, S4) were purified and analyzed by spectroscopy in the native dark state. Since only S1 and S4 had tuning effects in the range of interest, we combined coevolving adjacent site variants S1/S2, and S3/S4 and followed two distinct routes by successively adding variant sites creating triple mutants. Starting from a green-shifted BRh1 variant carrying S5 and S6, a third trajectory was studied where variant sites S1, S2, S4 were also successively added.

Wing reflectance

Reflectance spectra were measured from leaves of *Zamia integrifolia* leaves (Zamiacae) collected at the Montgomery Botanical Garden (Miami, FL, USA), and from *E. atala* discrete wing, thorax, and abdominal patches of coloured-scales from both males and females ($N_{individuals}$=3-5, 2 to 4 measurements per scale type, SI datafile 2), and in a Leitz Ortholux-Pol microscope equipped with a Leitz MPV-1 photometer with epi-illumination block, fitted with a Leitz 5.6X/0.15P objective. The illuminator filled the back focal plane of the objective with axial incident light. The photometer measured reflected light from the full aperture of the objective from a spot in the front focal plane that was 210 μm in diameter. Reflectance data were corrected for stray light by subtracting data measured

894 from the MSP objective viewing a light-dump comprised of substantially out-of-focus
895 black velvet cloth. Corrected reflectance data were normalized against the same
896 normalization constant of 0.179 to preserve relative brightnesses among all measured
897 body patches. Normalized reflectance data were analyzed in R (V.0.99.486) (100).
898

899 **Data accessibility**

900 Our sequencing data have been deposited in the GenBank database under accession
901 numbers MN831881-MN831887 and under SRA Bioproject XXXXX. Data for
902 photochemistry and optophysiological measurements, opsin absorbance spectra,
903 reflectance spectra and transcriptomics expression are available as supplementary files.

904 **Competing interests**

905 We declare no competing interests

906 **Acknowledgements**

907 We thank Masaru Hojo for providing eggs, larvae and pupae of *Arhopala japonica*, Maria
908 Eriksson and Peg Coughin for assistance with electron microscopy, Sara Jones and
909 Jonathan Schmidt-Burk for advice with cell culture, Ian Slaymaker for advice with protein
910 purification procedures, Rachel Gaudet and José Velilla for guidance using Pymol and
911 homology modeling, Rosalie Crouch for providing the 11-cis-retinal, Jeanne Serb and
912 Davide Faggionato for advice with cis-retinal delivery, Almut Kelber, Mandyam
913 Veerambudi Srinivasan, Mary Caswell Stoddard, Julien Ayroles, and Riannon Macrae for
914 helpful discussions and Richard Belliveau, Maggie Starvish and Rachel Hawkins for
915 providing logistical support. This work was supported by a Mind Brain Behavior
916 Interfaculty grant to NEP and MAL, an Alice and Knut Wallenberg Postdoctoral
917 fellowship at the Broad Institute of MIT and Harvard to MAL, a NSF Graduate
918 Research Fellowship to SSa, personal funds of GDB, and NSF DEB- 1541560 to NEP
919 and PHY-1411445 to NEP and NY.

920

921 **Figures and Tables**
922
923 **Figure 1. Long-wavelength photochemical difference spectra from lycaenid butterflies.**
924 Difference spectra (DS) were obtained following partial bleaches of long wavelength rhodopsins
925 from dorsal retina of intact butterflies. Datapoints represent absorbance differences between
926 amounts of Rhodopsin (R, green or red) and its Metarhodopsin photoproduct (M, blue) product
927 after a dark-period that followed photoconversion. Each black curve represents a computed
928 difference spectrum for least square fits estimates at *(A)* R570 of *Arhopala japonica*, *(B)* R562 of
929 *Eumaeus atala* and *(C)* R518 of *Callophrys sheridanii*. In *E. atala* the difference spectrum was
930 acquired upon complete degradation of the M photoproduct and with small contributions from
931 R440 and RBP395. In *Celastrina ladon*, λ_{max} of M and λ_{max} of R are very close, which pushed the
932 DS negative peak to the right. Photographs represent respective butterflies (left) and butterfly
933 eyeshine (right) in the dorsal retina (see also Fig. S1).
934
935 **Figure 2. *In vivo* evidence for four rhodopsins in the Atala hairstreak butterfly.** *(A)*
936 Photochemical analysis of a butterfly male eyeshine using an epi-microspectrophotometer. Log-
937 reflectance difference absorbance spectra (DS, Difference Spectrum, filled circles) and fitted
938 curves (solid line) measured from dark-adapted eyes via partial-bleaching experiments of R440.
939 *(B)* Optophysiological analyses designed to measure pupillary sensitivity in the UV. The least
940 squares fit analysis provides confident estimates for a UV rhodopsin with λ_{max} at 360nm.
941 Comparison to sensitivities in the blue, driven by R440 and in the red, driven by LW R565
942 rhodopsins, show that those two opsins make no contributions in the UV. *(C-D)* Densitometric
943 analysis of an epi-microspectrophotometric reflectance spectrum of a male *(C)* and female *(D).*
944 Completely dark-adapted *E. atala* eyeshine is used to confirm the contribution of each estimated
945 visual pigment in the eye. The black dots plot the log-reflectance spectrum. The red curve is the
946 spectrum after having computationally stripped optical density (OD) 1.50 of rhodopsin with λ_{max}
947 565 nm so that the residual spectrum is flat from 565 nm to 660 nm; cyan curve, the log-
948 reflectance spectrum after having stripped OD 0.36 of R440 to produce a residual flat from 450
949 nm. The black curve is the log-reflectance spectrum after stripping OD 0.72 for R395 and 0.55
950 R360, leaving a residual spectrum fit by a fourth-rhodopsin R495. The densitometric analysis of
951 female eyes *(D)* is qualitatively identical, with stripping densities of 1.55 R565, 0.40 R440, 0.80
952 RBP395 and 0.55 R350, leaving a residual indicative of a fourth pigment contribution, fit by
953 rhodopsin R495. Stripping the R495 residual leaves the curve plotted in open squares that is the
954 putative average log-reflectance spectrum of the tapetum, that is flat from the UV out to 660 nm.
955 *(E)* Computational analysis of male residual reflectance spectra supports the contribution of a
956 fourth opsin pigment with λ_{max} peaking around 495 nm. The residual fit for females is shown in the

957 inset. *(F)* Sensitivity data from an optophysiological threshold experiment measured at
958 wavelengths close to λ_{max} values (360 nm, 440 nm, 495 nm, 562 nm) of the four rhodopsins. This
959 shows that sensitivities at 440 nm and 495 nm cannot possibly be driven by R565.
960
961 **Figure 3. Functional characterization of red-shifted long wavelength lycaenid butterfly**
962 **opsins.** *(A)* Schematic of modified pCDNA expression vector cassette and workflow for functional
963 characterization of rhodopsin complexes with cis-retinal chromophore. All steps following addition
964 of cis-retinal are performed under dim red-light illumination. *(B)* Neighbour-Joining (NJ) tree of
965 butterfly long wavelength opsins. Bootstrap node support is as follows: 50-74%, white circle; 75-
966 94%, grey circle; ≥ 95%, black circle. Previously published λ_{max} physiological data are indicated in
967 parentheses when known (20, 27, 40, 41, 45). Corresponding family names are labeled on the
968 right. L, T and P correspond to lycaenid subfamilies Lycaeninae, Theclinae and Polyommatinae,
969 respectively. *(C-F)* Dark spectra of long wavelength rhodopsin (LWRh) expressed using an
970 HEKT293 transient cell culture system and purified via FLAG-epitope. LWRh rhodopsin
971 absorbance spectra are indicated with black dots (Table S7, Dataset S1), and a rhodopsin
972 template data (99) was computed to obtain the best estimates of λ_{max} fitting the data. (C)
973 *Arhopala japonica* purified LW opsin with λ_{max} = 570 nm, (D) *Eumaeus atala* purified LW opsin
974 with λ_{max} = 567 nm, *(E) Callophrys sheridanii* purified LW opsin with λ_{max} = 525 nm, (F) *Celastrina*
975 *ladon* purified LW opsin with λ_{max} = 525 nm.
976
977 **Figure 4**. **Anatomical overview of a typical ommatidium in *Eumaeus atala*.** *(A)* Diagram
978 illustrating a typical ommatidium and the relative contribution of nine photoreceptor cells R1-R9 at
979 different depths along the rhabdom (480 µm long). Photoreceptors R1 and R2 are proximal cells
980 in region *a* (126 µm) that contribute microvillar structures containing UVRh, BRh1 and BRh2
981 rhodopsins. Photoreceptors R3-R4 are proximal receptors containing LWRh and Brh1
982 rhodopsins. Photoreceptors R5-R8 are distal cells exclusively expressing the LWRh rhodopsin
983 (see also Fig 4, Fig S2). The basal cell, R9 is restricted to the region immediately proximal to the
984 basement membrane (460 µm, h). The expressed mRNA opsin type was not investigated in this
985 cell. *(B)* Scanning electron micrographs from a male dorsal eye region at 30° elevation across the
986 rhabdom. Scale bars, 2 µm. *(C)* Distal microvilli in regions *a- b* are exclusively oriented parallel to
987 the R1-R2 axis (left panel). As R3-R4 cells expand and contribute the majority of microvilli from
988 regions *c* to *e*, together with novel contributions from proximal receptors R5 to R8, three
989 ommatidia subtypes are formed that exhibit microvillar contributions parallel to (left panel) but
990 also intertwisted (middle panel) and perpendicular to the R1-R2 axis (right panel). Scale bars, 500

991 nm. *bm,* basement membrane*; rh,* rhabdom*; nc,* nucleus*; tp,* tapetum*; vc*, vacuole; 1-9,
992 photoreceptor cells R1 to R9.

993 **Figure 5. Adjacent photoreceptor localization between duplicate blue opsin mRNAs drives**
994 **retinal mosaic expansion.** Double fluorescent *in situ* hybridization shows six ommatidial types in
995 *E. atala* compared to ancestral butterfly eyes. *(A-F)* Exclusive one-cell one-mRNA expression
996 pattern in distal photoreceptors R1 and R2, showing for *(A*) UVRh (inset in *(D*)**,** *(B)* BRh1 mRNA
997 (inset in *(E*)) and *(C*) BRh2 mRNA (inset in *(F*)). Circles highlight the four distinct opsin expression
998 patterns in R1 and R2. *(G-I)* UVRh, BRh1 and BRh2 mRNAs do not coexpress in R1-R2 cells.
999 Photoreceptor cells R3-R8 express the LWRh opsin (red). Males and females show dorso-ventral
1000 dimorphism (Fig. S4). *(J)* Schematic representation of opsin-based photoreceptor classes in
1001 males and females of the six ommatidial types as follows (R1-R2-R3/R8): UV-UV-LW, UV-B1-
1002 LW, UV-B2-LW, B1-B1-LW, B1-B2-LW, B2-B2-LW.

1003 **Figure 6. Residues responsible for spectral tuning shifts in blue rhodopsins.** *(A)* NJ tree of
1004 selected lepidopteran blue opsin amino acid sequences. The squid rhodopsin, *Todarodes*
1005 *pacificus* (acc. nr. CAA49906) is used as outgroup. Bootstrap node support is as follows: 50-74%,
1006 white circle; 75-94%, grey circle; ≥ 95%, black circle. Dots above the partial multiple sequence
1007 alignment shows the 21 amino acid residues residing within 5 Å of any carbon atom in the retinal
1008 polyene chain. *Blue* dots identify the six positions where amino acid residues differ between *E.*
1009 *atala* BRh1 and BRh2, blue rectangles highlight variants at these positions in lycaenids. Residue
1010 numbering is based on residue position in the squid rhodopsin. Residues are coloured according
1011 to their physicochemical properties in Jalview v2 (104). Grey arrows indicate β-strands forming
1012 the binding pocket. *(B)* Blue opsin absorbance spectra (dots) fitted to the visual template (cyan
1013 and blue line functions), respectively. *(C)* Predicted structure for Eat-BRh1 based on homology
1014 modeling with the squid rhodopsin with variant sites Ala116, Iso120, GLy175, Phe177, Iso206.
1015 *(D)* Native Brh1 rhodopsin bearing S1 (A116), S2 (I120) and S4 (Y177). *(E)* Substituting residues
1016 116, 120 and 177 leads to a 30-nm partial blue-shift in rhodopsin absorbance λ_{max} in the triple
1017 mutant (see also Figure S2). This tuning shift may be mediated by several possible mechanisms
1018 including additive effects caused by novel hydrogen bond formation at the coevolving adjacent
1019 sites 116 and 120 *(F)* and with nearby conserved residues G115 and G121. *(G)* An alternative
1020 evolutionary route involves substituting G175S (S3) which partially compensates the green tuning
1021 shift of double mutant A116S/Y177F (Fig. S6, Table S8) and tunes the absorbance spectrum
1022 near 500nm. These alternative trajectories highlight additive and epistatic interactions between
1023 four residues at sites 1-4 *(F, H)* in the acquisition of the blue-shifted function.

1024

1025 **Figure 7. Wing and body spectral reflectance in *Eumaeus atala*.** *(A)* Female (F) and male (M)
1026 dorsal forewing (DFW), ventral hindwing (VHW), thorax and abdominal scales. The photographs
1027 below each wing are magnified views of representative coloured wing scales in patches
1028 measured by epi-microspectrophotometry (MSP). The field of view for each photograph is 210 μm
1029 in diameter. Photographs were acquired using an Olympus TG-1 camera set at zoom 2.8. *(B-C)*
1030 Graphs of mean reflectance spectra ± standard errors of the mean of wing scale patches *(B)* and
1031 body scales *(C)* (N=3-5 individuals per sex). *(D)* Leaf reflectance spectra (4-5 measurements per
1032 leaf surface) (SI Datafile 2). *(E) E. atala* rhodopsin absorbance spectra. Male and female wing
1033 reflectance spectra are not exclusive, and spectral shapes are highly consistent indicating that
1034 male and female spectra are similar in the visible. In females, hindwing cyan spots show a
1035 reflectance peak at 540 nm *(B)*. Blue scales on the thorax and dorsal forewings have a
1036 reflectance peak at 490-500 nm. Hindwing *(B)* and abdominal red patches *(C)* have identical high
1037 reflectance spectra at long wavelengths in both sexes. MSP analyses from black areas of ventral
1038 hindwings *(B)* showed that black scales are only 1 % as reflective as adjacent cyan scales in the
1039 blue/green band. Brightness in black regions decreases 100-fold compared to adjacent cyan
1040 scales in both sexes. All reflectance curves overlap at contributing wavelengths for at least two
1041 rhodopsins, thereby efficiently distinguishing foliage and sex-specific wing colour patterns.

1042

1043 **References**

1044 1. M. Lynch, J. S. Conery, The evolutionary fate and consequences of duplicate genes.
1045 *Science* **290**, 1151-1155 (2000).

1046 2. H. Kaessmann, Origins, evolution, and phenotypic impact of new genes. *Genome*
1047 *research* **20**, 1313-1326 (2010).

1048 3. M. Long, K. Thornton, Gene duplication and Evolution. *Nature* **293**, 1551a (2001).

1049 4. J. Zhang, Evolution by gene duplication: an update. *Trends in Ecology & Evolution* **18**,
1050 292-298 (2003).

1051 5. M. A. Liénard, H.-L. Wang, J.-M. Lassance, C. Löfstedt, Sex pheromone biosynthetic
1052 pathways are conserved between moths and the butterfly *Bicyclus anynana*. *Nat Comms* **5:3957**
1053 (2014).

1054 6. R. Feuda, F. Marlétaz, M. A. Bentley, P. W. H. Holland, Conservation, Duplication, and
1055 Divergence of Five Opsin Genes in Insect Evolution. *Genome biology and evolution* **8**, 579-587
1056 (2016).

1057 7. P. Brand *et al.*, The evolution of sexual signaling is linked to odorant receptor tuning in
1058 perfume-collecting orchid bees. *Nature Communications* **11**, 244 (2020).

1059 8. M. Chapal, S. Mintzer, S. Brodsky, M. Carmi, N. Barkai, Resolving noise–control conflict
1060 by gene duplication. *PLOS Biology* **17**, e3000289 (2019).

1061 9. M. Soskine, D. S. Tawfik, Mutational effects and the evolution of new protein functions.
1062 *Nature Reviews Genetics* **11**, 572-582 (2010).

1063 10. J. Zhang, Y. Zhang, H. Rosenberg, Adaptive evolution of a duplicated pancreatic
1064 ribonuclease gene in a leaf-eating monkey. *Nature Genetics* **30**, 411-415 (2002).

1065 11. G. M. Castiglione, B. S. W. Chang, Functional trade-offs and environmental variation
1066 shaped ancient trajectories in the evolution of dim-light vision. *eLife* **7**, e35957 (2018).

1067 12. M. Manceau, V. Domingues, C. Linnen, E. Rosenblum, H. Hoekstra, Convergence in
1068 pigmentation at multiple levels: mutations, genes and function. *Philos Trans R Soc Lond B Biol*
1069 *Sci* **365**, 2439-2450 (2010).

1070 13. S. B. Carroll, Evolution at Two Levels: On Genes and Form. *PLOS Biology* **3**, e245
1071 (2005).

1072 14. F. Hauser, B. Chang, Insights into visual pigment adaptation and diversity from model
1073 ecological and evolutionary systems. *Current opinion in genetics & development* **47**, 110-120
1074 (2017).

1075 15. A. Terakita, The opsins. *Protein family review* **6**, 213 (2005).

1076 16. S. Yokoyama, Evolution of Dim-Light and Color Vision Pigments. *Annu Rev Genom Hum*
1077 *G* **9**, 259-282 (2008).

1078 17. D. E. Nilsson, M. F. Land, J. Howard, Optics of the butterfly eye. *Journal of Comparative*
1079 *Physiology A* **162**, 341-366 (1988).

1080 18. A. D. Briscoe, L. Chittka, The evolution of color vision in insects. *Ann Rev Entomol* **46**,
1081 471-510 (2001).

1082 19. G. Bernard, C. Remington, Color vision in *Lycaena* butterflies: spectral tuning of receptor
1083 arrays in relation to behavioral ecology. *Proc Nat Acad Sci USA* **88**, 2783-2787 (1991).

1084 20. F. Frentiu, G. Bernard, M. Sison-Mangus, A. Van Zandt Brower, A. Briscoe, Gene
1085 Duplication Is an Evolutionary Mechanism for Expanding Spectral Diversity in the Long-
1086 Wavelength Photopigments of Butterflies. *Mol Biol Evol* **24**, 2016-2028 (2007).

1087 21. A. D. Briscoe *et al.*, Positive selection of a duplicated UV-sensitive visual pigment
1088 coincides with wing pigment evolution in Heliconius butterflies. *PNAS* **107**, 3628-3633 (2010).

1089 22. D. Armisén *et al.*, The genome of the water strider Gerris buenoi reveals expansions of
1090 gene repertoires associated with adaptations to life on the water. *BMC Genomics* **19**, 832 (2018).

1091 23. C. R. Sharkey *et al.*, Overcoming the loss of blue sensitivity through opsin duplication in
1092 the largest animal group, beetles. *Scientific Reports* **7**, 8 (2017).

1093 24. H. Koshitaka, M. Kinoshita, M. Vorobyev, K. Arikawa, Tetrachromacy in a butterfly that
1094 has eight varieties of spectral receptors. *Proc Biol Sci* **275**, 947-954 (2008).

1095 25. F. D. Frentiu *et al.*, Adaptive evolution of color vision as seen through the eyes of
1096 butterflies. *PNAS* **104**, 8634-8640 (2007).

1097 26. R. Futahashi *et al.*, Extraordinary diversity of visual opsin genes in dragonflies. *PNAS*
1098 **112**, E1247 (2015).

1099 27. M. Wakakuwa *et al.*, Evolution and Mechanism of Spectral Tuning of Blue-Absorbing
1100 Visual Pigments in Butterflies. *PLOS ONE* **5**, e15015 (2010).

1101 28. F. E. Hauser, I. v. Hazel, B. S. W. Chang, Spectral tuning in vertebrate short wavelength-
1102 sensitive 1 (SWS1) visual pigments: Can wavelength sensitivity be inferred from sequence data?
1103 *J Exp Zool* **322**, 529-539 (2014).

1104 29. M. Perry *et al.*, Molecular logic behind the three-way stochastic choices that expand
1105 butterfly colour vision. *Nature* **535**, 280-284 (2016).

1106 30. A. D. Briscoe, Reconstructing the ancestral butterfly eye: focus on the opsins. *J Exp Biol*
1107 **211**, 1805-1813 (2008).

1108 31. K. Arikawa, The eyes and vision of butterflies. *J Physiol* **595**, 5457-5464 (2017).

1109 32. G. H. Jacobs, Primate photopigments and primate color vision. *Proceedings of the*
1110 *National Academy of Sciences* **93**, 577 (1996).

1111 33. M. Luehrmann *et al.*, Short-term colour vision plasticity on the reef: changes in opsin
1112 expression under varying light conditions differ between ecologically distinct fish species. *The*
1113 *Journal of Experimental Biology* **221**, jeb175281 (2018).

1114 34. G. H. Jacobs, Evolution of colour vision in mammals. *Philos Trans R Soc B* **364**, 2957-
1115 2967 (2009).

1116 35. Y. Shichida, T. Matsuyama, Evolution of opsins and phototransduction. *Philos Trans R*
1117 *Soc B* **364**, 2881 (2009).

1118 36. A. Gutierrez Eduardo de *et al.*, The role of ecological factors in shaping bat cone opsin
1119 evolution. *Proc Biol Sci* **285** (2018).

1120 37. A. Monteiro, Origin, Development, and Evolution of Butterfly Eyespots. *Annual Review of*
1121 *Entomology* **60**, 253-271 (2015).

1122 38. K. Dasmahapatra *et al.*, Butterfly genome reveals promiscuous exchange of mimicry
1123 adaptations among species. *Nature* **487**, 94-98 (2012).

1124 39. N. P. Lord *et al.*, A cure for the blues: opsin duplication and subfunctionalization for short-
1125 wavelength sensitivity in jewel beetles (Coleoptera: Buprestidae). *BMC Evolutionary Biology* **16**,
1126 107 (2016).

1127 40. M. P. Sison-Mangus, A. D. Briscoe, G. Zaccardi, H. Knüttel, A. Kelber, The lycaenid
1128 butterfly Polyommatus icarus; uses a duplicated blue opsin to see green. *Journal of Experimental*
1129 *Biology* **211**, 361 (2008).

1130 41. M. P. Sison-Mangus, G. D. Bernard, J. Lampel, A. D. Briscoe, Beauty in the eye of the
1131 beholder: the two blue opsins of lycaenid butterflies and the opsin gene-driven evolution of
1132 sexually dimorphic eyes. *J Exp Biol* **209**, 3079-3090 (2006).

1133 42. H. Awata, M. Wakakuwa, K. Arikawa, Evolution of color vision in pierid butterflies: blue
1134 opsin duplication, ommatidial heterogeneity and eye regionalization in Colias erate. *Journal of*
1135 *Comparative Physiology A* **195**, 401-408 (2009).

1136 43. P. Chauhan *et al.*, De novo transcriptome of Ischnura elegans provides insights into
1137 sensory biology, colour and vision genes. *BMC Genomics* **15**, 808 (2014).

1138 44. A. Briscoe, Six opsins from the butterfly *Papilio glaucus*: molecular phylogenetic evidence
1139 for paralogous origins of red-sensitive visual pigments in insects. *Journal of Molecular Evolution*
1140 **51**, 110-121 (2000).

1141 45. K. Arikawa, Spectral organization of the eye of a butterfly, *Papilio*. *J Comp Physiol* **189**,
1142 791-800 (2003).

1143 46. P.-J. Chen, H. Awata, A. Matsushita, E.-C. Yang, K. Arikawa, Extreme Spectral Richness
1144 in the Eye of the Common Bluebottle Butterfly, Graphium sarpedon. *Front Ecol Evol* **4**, 18 (2016).

1145 47. G. Pratt, J. Emmel, G. D. Bernard, The Buckwheat Metalmarks. *Am Butterflies* **19**, 4-31
1146 (2011).

1147 48. M. Wakakuwa, D. G. Stavenga, M. Kurasawa, K. Arikawa, A unique visual pigment
1148 expressed in green, red and deep-red receptors in the eye of the small white butterfly, *Pieris*
1149 *rapae crucivora*. *J Exp Biol* **207**, 2803-2810 (2004).

1150 49. Y. Ogawa, M. Kinoshita, D. G. Stavenga, K. Arikawa, Sex-specific retinal pigmentation
1151 results in sexually dimorphic long-wavelength-sensitive photoreceptors in the eastern pale

1152 clouded yellow butterfly, <em>Colias erate</em&gt. *The Journal of Experimental Biology*
1153 **216**, 1916 (2013).

1154 50. A. Satoh *et al.*, Red-shift of spectral sensitivity due to screening pigment migration in the
1155 eyes of

1156 a moth, Adoxophyes orana. *Zool Lett* **3**, 14 (2017).

1157 51. P. Pirih *et al.*, The giant butterfly-moth Paysandisia archon has spectrally rich apposition
1158 eyes with unique light-dependent photoreceptor dynamics. *Journal of Comparative Physiology A*
1159 **204**, 639-651 (2018).

1160 52. G. Bernard, Red-absorbing Visual Pigment of Butterflies. *Science* **203**, 1125-1127
1161 (1979).

1162 53. G. Zaccardi, A. Kelber, M. P. Sison-Mangus, A. D. Briscoe, Color discrimination in the red
1163 range with only one long-wavelength sensitive opsin. *J Exp Biol* **209**, 1944-1955 (2006).

1164 54. G. D. Bernard, Bleaching of rhabdoms in eyes of intact butterflies. *Science* **219**, 69-71
1165 (1983).

1166 55. S. Yokoyama *et al.*, Epistatic Adaptive Evolution of Human Color Vision. *PLOS Genetics*
1167 **10**, e1004884 (2014).

1168 56. M. Neitz, J. Neitz, G. H. Jacobs, Spectral tuning of pigments underlying red-green color
1169 vision. *Science* **252**, 971 (1991).

1170 57. Dulai KS, v. D. M, M. JD, H. DM, *Genome Res* **9**, 629-638 (1999).

1171 58. S. Kawamura, Kawamura S. Color vision diversity and significance in primates inferred
1172 from genetic and field studies. Genes Genomics. 2016;38:779–791. doi:10.1007/s13258-016-
1173 0448-9. *Genes Genomics* **38**, 779-791 (2016).

1174 59. A. Kelber, Bird colour vision - from cones to perception. *Current opinion in Behavioral*
1175 *Sciences* **30**, 34-40 (2019).

1176 60. A. Terakita *et al.*, Expression and comparative characterization of Gq-coupled
1177 invertebrate visual pigments and melanopsin. *J Neurochem* **105**, 883-890 (2008).

1178 61. F. Frentiu *et al.*, Clines in butterflies suggest novel roles for insect photopigments. *Mol*
1179 *Biol Evol* **32**, 368-379 (2014).

1180 62. T. Saito *et al.*, Spectral tuning mediated by helix III in butterfly long wavelength-sensitive
1181 visual opsins revealed by heterologous action spectroscopy. *Zoological Letters* **5**, 35 (2019).

1182 63. M. Wakakuwa, F. Stewart, Y. Matsumoto, S. Matsunaga, K. Arikawa, Physiological basis
1183 of phototaxis to near-infrared light in *Nephotettix cincticeps*. *Journal of Comparative Physiology A*
1184 **200**, 527-536 (2014).

1185 64. A. Kelber, Ovipositing butterflies use a red receptor to see green. *J Exp Biol* **202**, 2619-
1186 2630 (1999).

1187 65. R. Cannon, *Courtship and mating in butterflies: reproduction, mating, behaviour and*
1188 *sexual conflicts*. R. J. C. Cannon, Ed. (Severn, Gloucester, UK, 2020), pp. 376.

1189 66. M. Heikkilä, L. Kaila, M. Mutanen, C. Pena, N. Wahlberg, Cretaceous origin and repeated
1190 tertiary diversification of the redefined butterflies. *Proceedings of the Royal Society of London,*
1191 *Series B: Biological Sciences* **279**, 1093-1099 (2012).

1192 67. M. Espeland *et al.*, A Comprehensive and Dated Phylogenomic Analysis of Butterflies.
1193 *Cur Biol* **28**, 770-778.e775 (2018).

1194 68. S. Koi, D. Hall, Atala Butterfly, Atala Hairstreak, Coontie Hairstreak, *Eumaeus atala* Poey
1195 1832 (Insecta: Lepidoptera: Lycaenidae). (2016).

1196 69. A. Myrberg, M. Mohler, J. Catala, Sound production by males of a coral reef fish
1197 (*Pomacentrus partitus*): its significance to females. *Animal Behaviour* **34** (1986).

1198 70. D. Faggionato, J. M. Serb, Strategy to Identify and Test Putative Light Sensitive Non-
1199 Opsin G-Protein-Coupled Receptors: A Case Study. *Biol. Bull.* **233**, 70-82 (2017).

1200 71. J. Morrow, B. Chang, The p1D4-hrGFP II expression vector: A tool for expressing

1201 and purifying visual pigments and other G protein-coupled receptors. *Plasmid* **64**, 162-169
1202 (2010).

1203 72. M. Murakami, T. Kouyama, Crystal structure of squid rhodopsin. *Nature* **453**, 363 (2008).

1204 73. A. Kelber, L. S. V. Roth, Nocturnal colour vision – not as rare as we might think. *J Exp*
1205 *Biol* **209**, 781 (2006).

1206 74. J. Fasick, N. Lee, D. Oprian, Spectral tuning in the human blue cone pigment.
1207 *Biochemistry* **38**, 11593-11596 (1999).

1208 75. B. Wilts, H. Leertouwer, D. G. Stavenga, Imaging scatterometry and
1209 microspectrophotometry of lycaenid butterfly wing scales with perforated multilayers. *J R Soc*
1210 *Interface* **6**, S185-S192 (2009).

1211 76. D. G. Stavenga, H. Leertouwer, P. Pirih, M. Wehling, Imaging scatterometry of butterfly
1212 wing scales. *Optics Express* **17**, 193-202 (2009).

1213 77. R. Vane-Wright, M. Boppre, Visual and chemical signalling in butterflies: functional and
1214 phylogenetic perspectives. *Proceedings of the Royal Society B Biological Sciences* **340**, 197-205
1215 (1993).

1216 78. J. A. Fordyce, C. C. Nice, M. L. Forister, A. M. Shapiro, The significance of wing pattern
1217 diversity in the Lycaenidae: mate discrimination by two recently diverged species. *Journal of*
1218 *Evolutionary Biology* **15**, 871-879 (2002).

1219 79. C. Jiggins, R. Naisbit, R. Coe, J. Mallet, Reproductive isolation caused by colour pattern
1220 mimicry. *Nature* **411**, 302-305 (2001).

1221 80. L. Wilkins, D. Osorio, Object colours, material properties and animal signals. *The Journal*
1222 *of Experimental Biology* 10.1242/jeb.204487, jeb.204487 (2019).

1223 81. J. Schnapf, T. Kraft, D. Baylor, Spectral sensitivity of human cone photoreceptors. *Nature*
1224 **325**, 439-441 (1987).

1225 82. M. Imafuku, I. Shimizu, H. Imai, Y. Shichida, Sexual difference in color sense in a
1226 lycaenid butterfly, *Narathura japonica*. *Zoolog Sci* **24**, 611-613 (2007).

1227 83. D. McCoy, R. Prum, Convergent evolution of super black plumage near bright color in 15
1228 bird families. *J Exp Biol* **222**, Pt 18 (2019).

1229 84. D. McCoy *et al.*, Structurally assisted super black in colourful peacock spiders. *Proc Biol*
1230 *Sci* **286**, 20190589 (2019).

1231 85. A. L. Davis, H. F. Nijhout, S. Johnsen, Diverse nanostructures underlie thin ultra-black
1232 scales in butterflies. *Nature Communications* **11**, 1294 (2020).

1233 86. O. Liew, P. Chong, B. Li, A. Asundi, Signature Optical Cues: Emerging Technologies for
1234 Monitoring Plant Health. *Sensors* **8**, 3205-3239 (2008).

1235 87. M. Rossi *et al.*, Neural processing genes are linked to divergence in visual mate
1236 preference in sympatric Heliconius butterflies. *bioRxiv*
1237 10.1101/2020.03.22.002121, 2020.2003.2022.002121 (2020).

1238 88. D. Osorio, M. Vorobyev, A review of the evolution of animal colour vision and visual
1239 communication signals. *Vision Research* **48**, 2042-2051 (2008).

1240 89. G. D. Bernard, Dark-Processes Following Photoconversion of Butterfly Rhodopsins.
1241 *Biophysics of Structure and Mechanism* **9**, 277-286 (1983).

1242 90. D. G. Stavenga, J. Numan, J. Tinbergen, J. Kuiper, Insect pupil mechanisms. II. Pigment
1243 migration in retinula cells of butterflies. *J Comp Phys A* **113**, 73-93 (1977).

1244 91. G. D. Bernard, "Noninvasive optical techniques for probing insect photoreceptors" in
1245 Biomembranes Part H: Visual pigments and purple membranes I, Methods in Enzymology, P. L,
1246 Ed. (Academic Press, New York, 1982), vol. 81, pp. 752-759.

1247 92. A. Briscoe, G. D. Bernard, A. Szeto, L. Nagy, R. White, Not all butterfly eyes are created
1248 equal: Rhodopsin absorption spectra, molecular identification, and localization of ultraviolet-, blue-
1249 , and green-sensitive rhodopsin-encoding mRNAs in the retina of Vanessa cardui. *J Comp Neurol*
1250 **458**, 334-349 (2003).

1251 93. F. Krueger, "Trim galore." A wrapper tool around Cutadapt and FastQC to consistently
1252 apply quality and adapter trimming to FastQ files. **516**, 517 (2015).

1253 94. B. J. Haas *et al.*, De novo transcript sequence reconstruction from RNA-seq using the
1254 Trinity platform for reference generation and analysis. *Nat Prot* **8**, 1494-1512 (2013).

1255 95. N. Bray, H. Pimentel, P. Melsted, L. Pachter, Near-optimal probabilistic RNA-seq
1256 quantification. *Nature Biotechnology* **34**, 525-527 (2016).

1257 96. S. F. Altschul *et al.*, Gapped BLAST and PSI-BLAST: a new generation of protein
1258 database search programs. *Nucleic Acids Research* **25**, 3389-3402 (1997).

1259 97. M. Kearse *et al.*, Geneious Basic: An integrated and extendable desktop software
1260 platform for the organization and analysis of sequence data. *Bioinformatics* **28**, 1647-1649
1261 (2012).

1262 98. A. Stamatakis, RAxML version 8: a tool for phylogenetic analysis and post-analysis of
1263 large phylogenies. *Bioinformatics* **30**, 1312-1313 (2014).

1264 99. A. Palacios, T. Goldsmith, G. D. Bernard, Sensitivity of cones from a cyprinid fish (Danio
1265 aequipinnatus) to ultraviolet and visible light. *Vis Neurosci* **13**, 411-421 (1996).

1266 100. R. C. Team, R: A language and environment for statistical computing. R Foundation for
1267 Statistical

1268 Computing, Vienna, Austria. URL https://www.R-project.org/. (2015).

1269 101. Y. Isogai *et al.*, Molecular organization of vomeronasal chemoreception. *Nature* **478**, 241-
1270 245 (2011).

1271 102. A. Waterhouse *et al.*, SWISS-MODEL: homology modelling of protein structures and
1272 complexes. *Nucleic acids research* **46**, W296-W303 (2018).

1273 103. Anonymous (The PyMOL Molecular Graphics System, Version 1.8, Schrödinger, LLC.

1274 104. A. M. Waterhouse, J. B. Procter, D. M. A. Martin, M. Clamp, G. J. Barton, Jalview version
1275 2: A Multiple Sequence Alignment and Analysis Workbench. *Bioinformatics* **25**, 1189-1191
1276 (2009).

1277

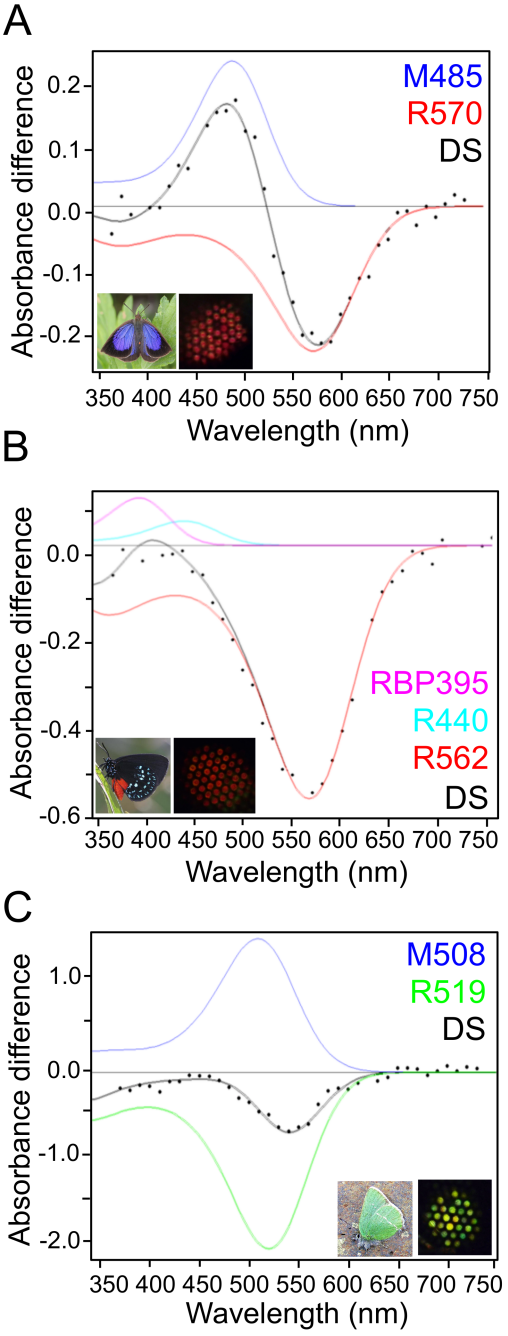
A
M485
R570
DS
Absorbance difference
0.2
0.1
0.0
-0.1
-0.2
350 400 450 500 550 600 650 700 750
Wavelength (nm)
B
RBP395
R440
R562
DS
Absorbance difference
0.0
-0.2
-0.4
-0.6
350 400 450 500 550 600 650 700 750
Wavelength (nm)
C
M508
R519
DS
Absorbance difference
1.0
0.0
-1.0
-2.0
350 400 450 500 550 600 650 700 750
Wavelength (nm)

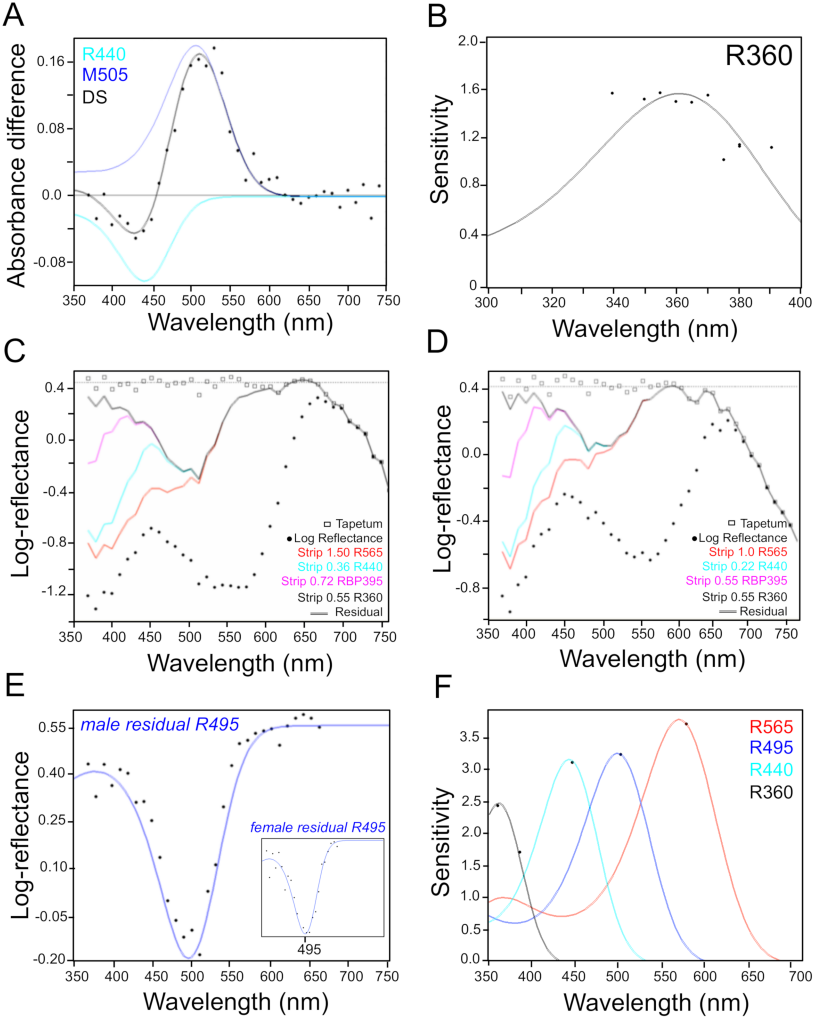
A
R440
M505
DS
Absorbance difference
Wavelength (nm)
B
R360
Sensitivity
Wavelength (nm)
C
Tapetum
Log Reflectance
Strip 1.50 R565
Strip 0.36 R440
Strip 0.72 RBP395
Strip 0.55 R360
Residual
Log-reflectance
Wavelength (nm)
D
Tapetum
Log Reflectance
Strip 1.0 R565
Strip 0.22 R440
Strip 0.55 RBP395
Strip 0.55 R360
Residual
Log-reflectance
Wavelength (nm)
E
male residual R495
female residual R495
495
Log-reflectance
Wavelength (nm)
F
R565
R495
R440
R360
Sensitivity
Wavelength (nm)

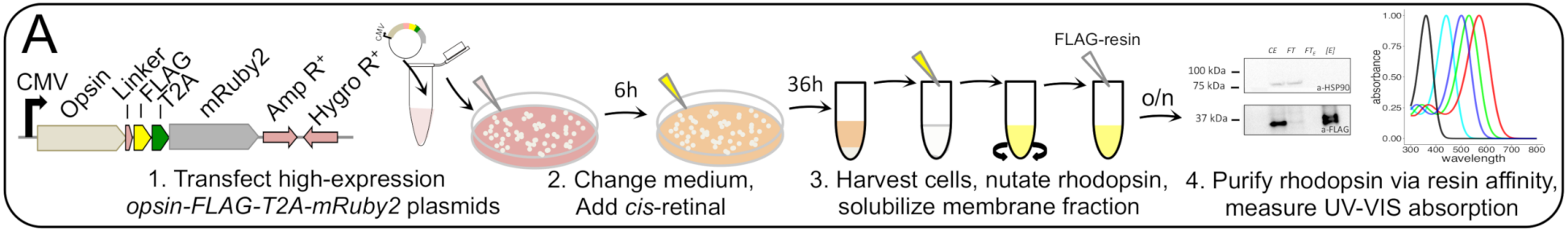
A
CMV
Opsin
Linker
FLAG
T2A
mRuby2
Amp R+
Hygro R+
6h
36h
FLAG-resin
o/n
100 kDa
75 kDa
37 kDa
a-HSP90
a-FLAG
absorbance
wavelength
1. Transfect high-expression opsin-FLAG-T2A-mRuby2 plasmids
2. Change medium, Add cis-retinal
3. Harvest cells, nutate rhodopsin, solubilize membrane fraction
4. Purify rhodopsin via resin affinity, measure UV-VIS absorption

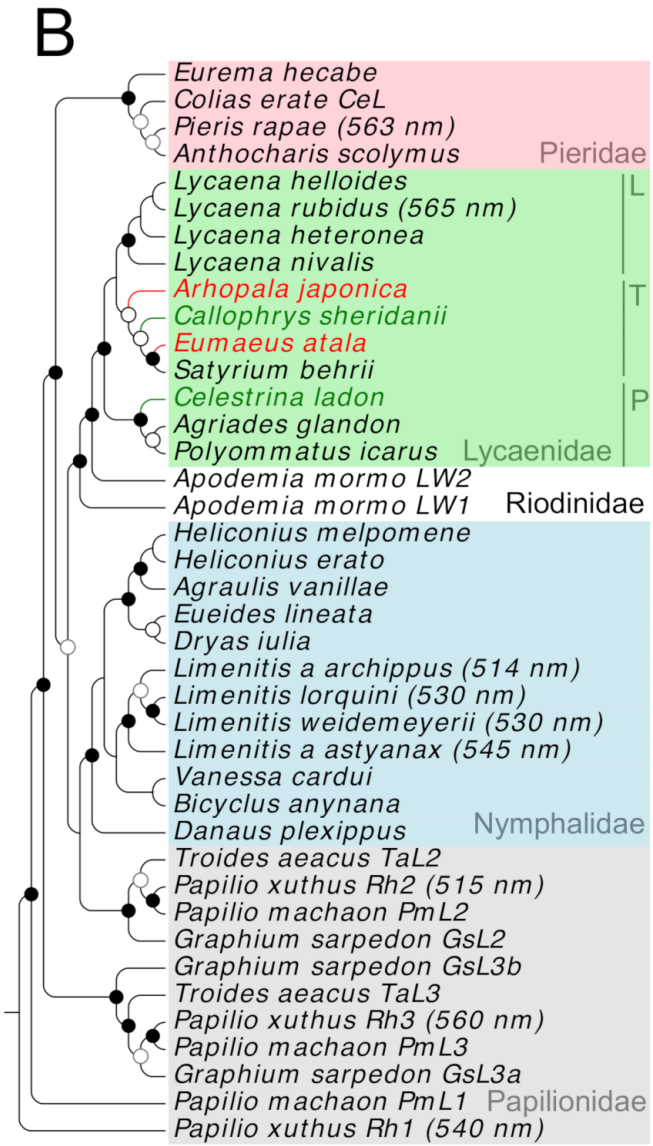
B
Eurema hecabe
Colias erate CeL
Pieris rapae (563 nm)
Anthocharis scolymus
Pieridae
Lycaena helloides
Lycaena rubidus (565 nm)
Lycaena heteronea
Lycaena nivalis
Arhopala japonica
Callophrys sheridanii
Eumaeus atala
Satyrium behrii
Celestrina ladon
Agriades glandon
Polyommatus icarus
Lycaenidae
L
T
P
Apodemia mormo LW2
Apodemia mormo LW1
Riodinidae
Heliconius melpomene
Heliconius erato
Agraulis vanillae
Eueides lineata
Dryas iulia
Limenitis a archippus (514 nm)
Limenitis lorquini (530 nm)
Limenitis weidemeyerii (530 nm)
Limenitis a astyanax (545 nm)
Vanessa cardui
Bicyclus anynana
Danaus plexippus
Nymphalidae
Troides aeacus TaL2
Papilio xuthus Rh2 (515 nm)
Papilio machaon PmL2
Graphium sarpedon GsL2
Graphium sarpedon GsL3b
Troides aeacus TaL3
Papilio xuthus Rh3 (560 nm)
Papilio machaon PmL3
Graphium sarpedon GsL3a
Papilio machaon PmL1
Papilionidae
Papilio xuthus Rh1 (540 nm)

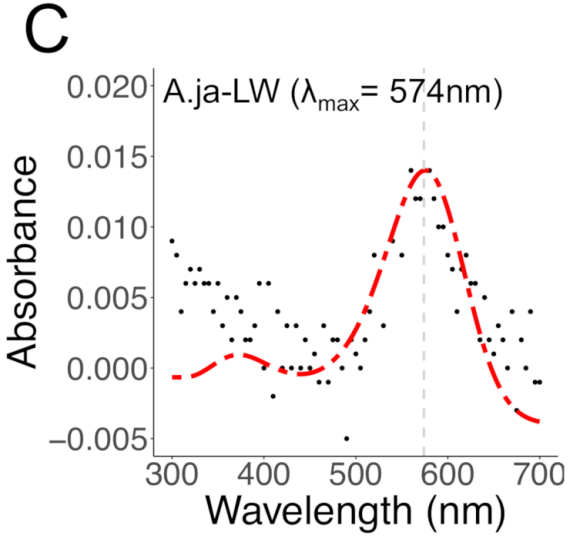
C
A.ja-LW (λmax= 574nm)
Absorbance
Wavelength (nm)

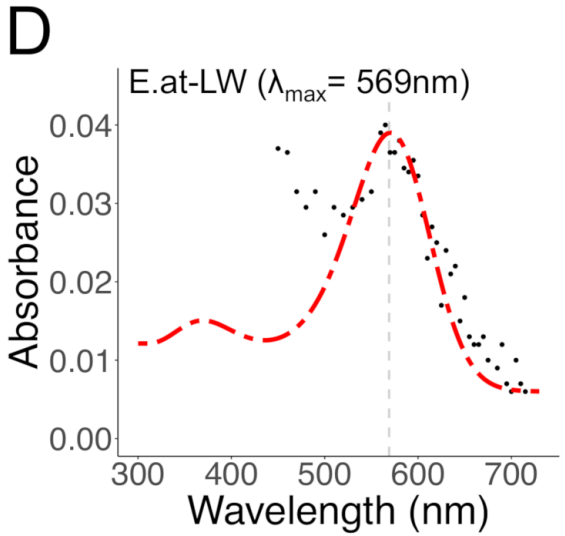
D
E.at-LW (λmax= 569nm)
Absorbance
Wavelength (nm)

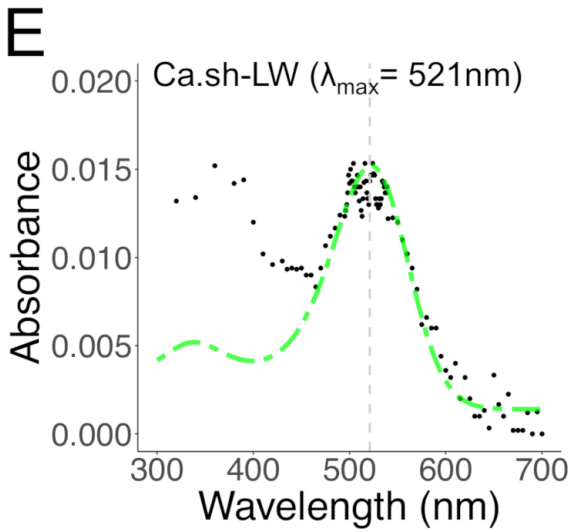
E
Ca.sh-LW (λmax= 521nm)
Absorbance
Wavelength (nm)

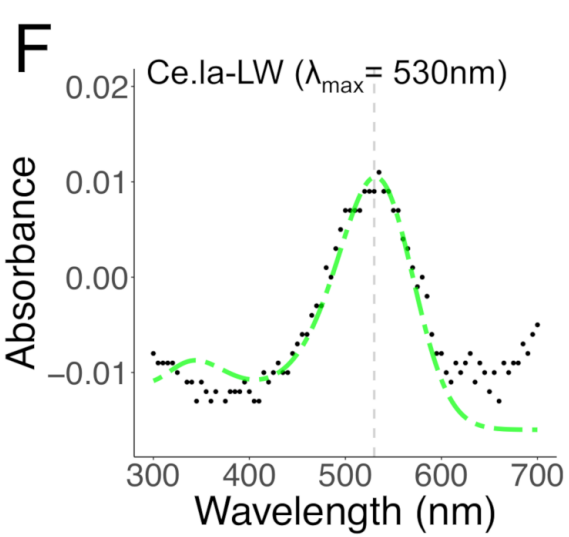
F
Ce.la-LW (λmax= 530nm)
Absorbance
Wavelength (nm)

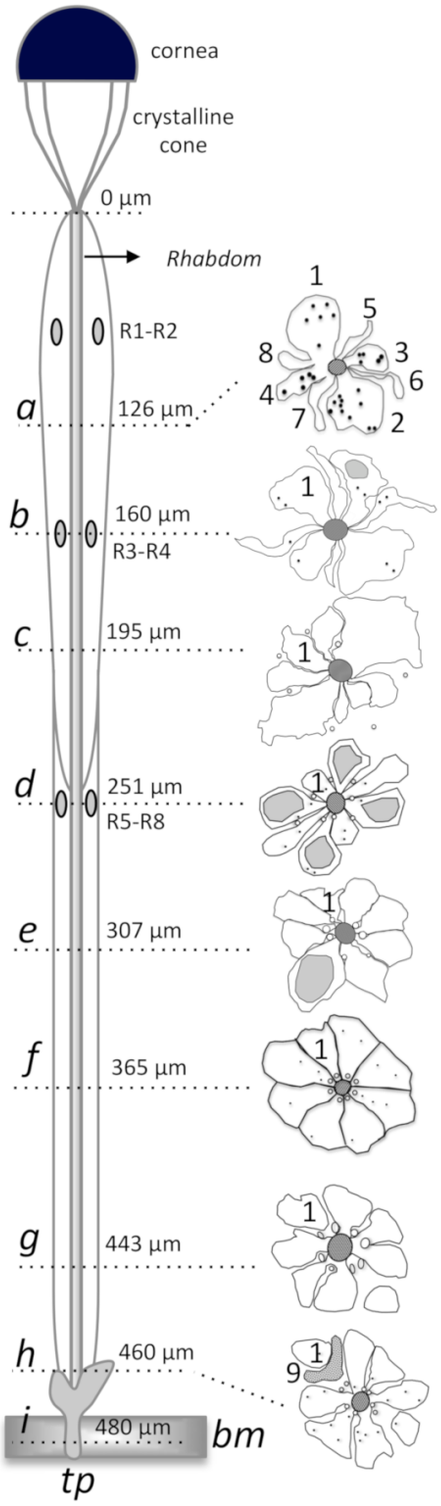
A
cornea
crystalline cone
0 µm
Rhabdom
R1-R2
a
126 µm
b
160 µm
R3-R4
c
195 µm
d
251 µm
R5-R8
e
307 µm
f
365 µm
g
443 µm
h
460 µm
i
480 µm
bm
tp

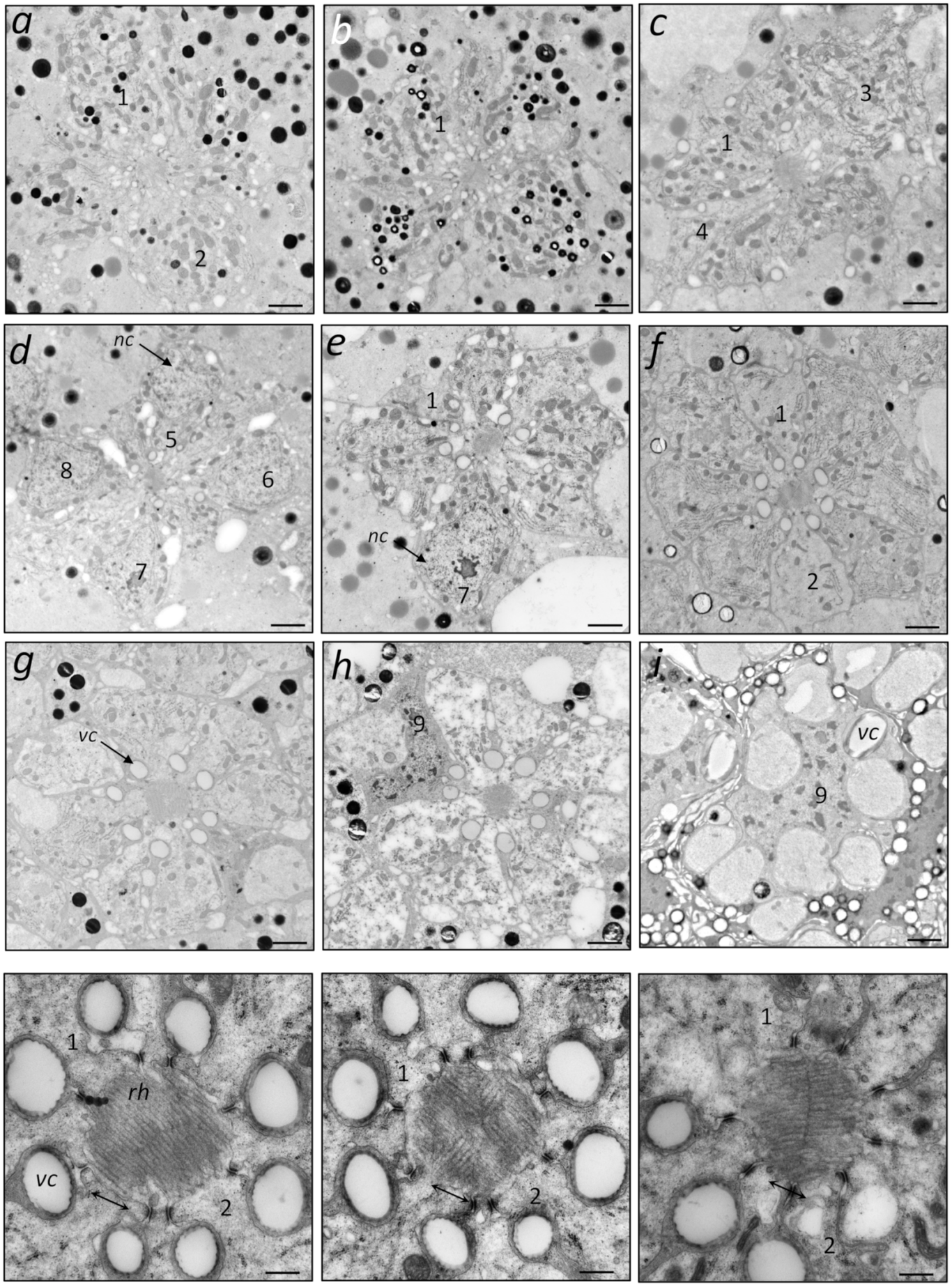
B
a
b
c
d
nc
e
nc
f
g
vc
h
i
vc
C
rh
vc

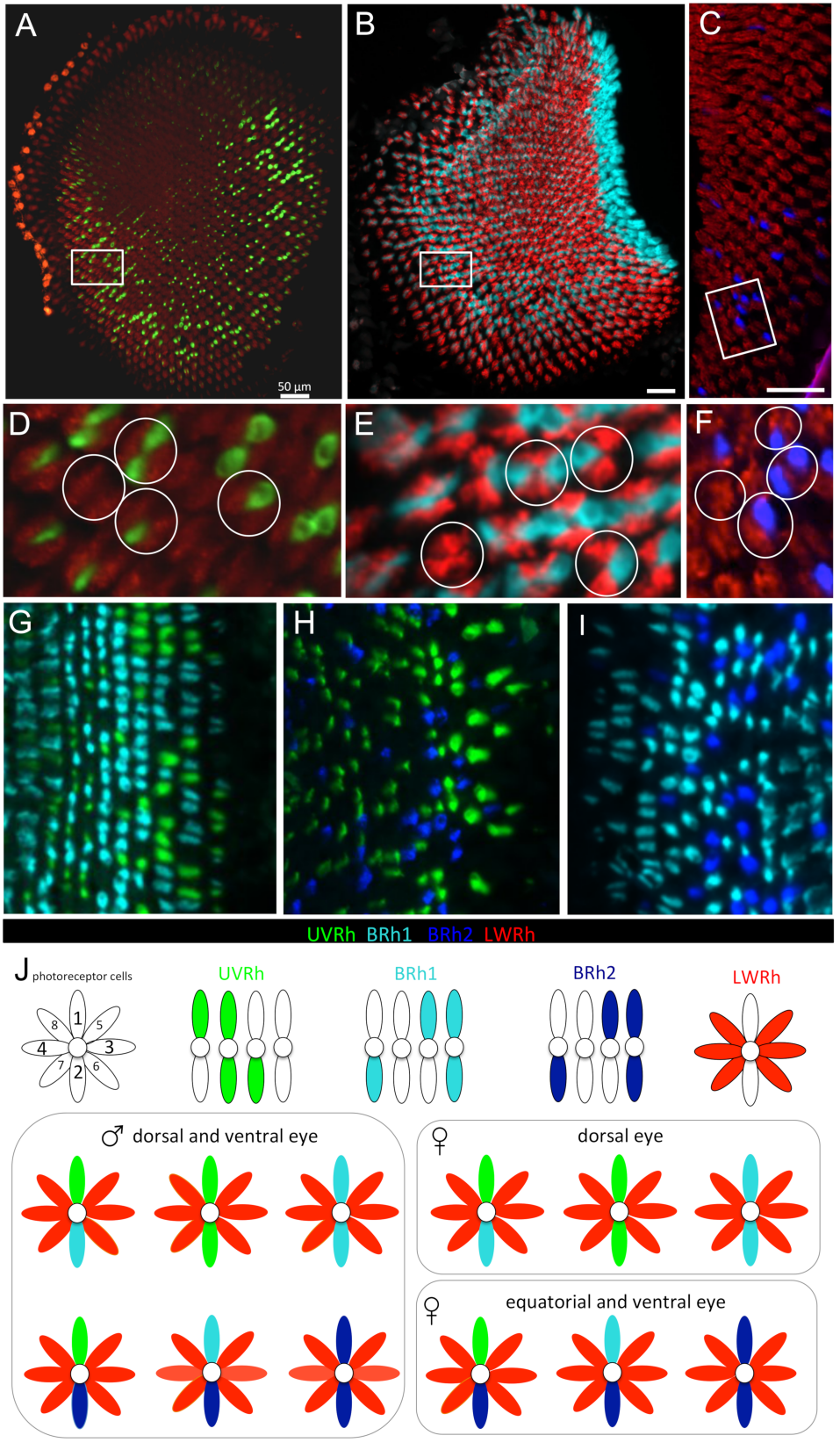
A
B
C
50 µm
D
E
F
G
H
I
UVRh BRh1 BRh2 LWRh
J photoreceptor cells
1
2
3
4
5
6
7
8
UVRh
BRh1
BRh2
LWRh
♂ dorsal and ventral eye
♀ dorsal eye
♀ equatorial and ventral eye

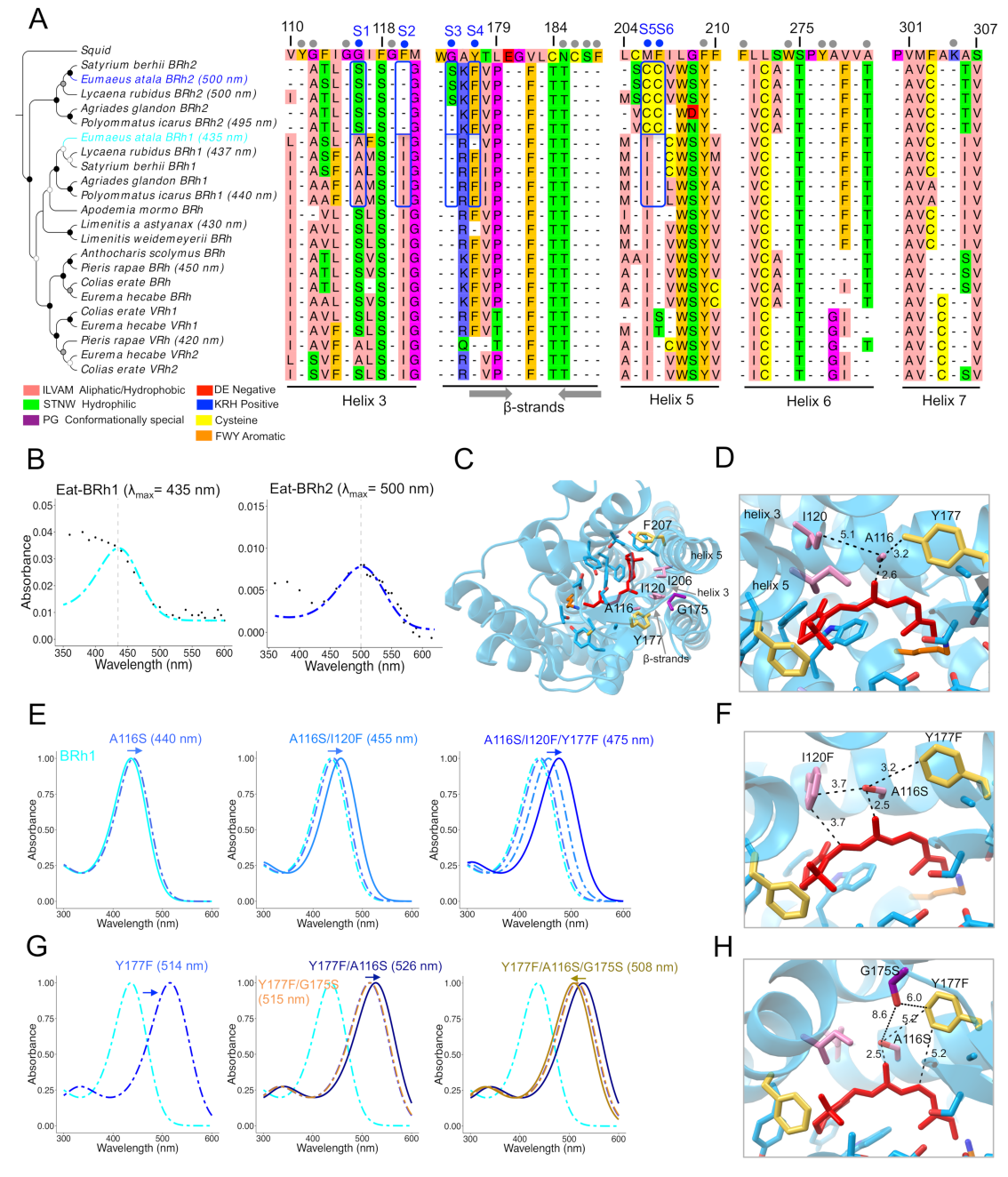
A
Squid
Satyrium berhii BRh2
Eumaeus atala BRh2 (500 nm)
Lycaena rubidus BRh2 (500 nm)
Agriades glandon BRh2
Polyommatus icarus BRh2 (495 nm)
Eumaeus atala BRh1 (435 nm)
Lycaena rubidus BRh1 (437 nm)
Satyrium berhii BRh1
Agriades glandon BRh1
Polyommatus icarus BRh1 (440 nm)
Apodemia mormo BRh
Limenitis a astyanax (430 nm)
Limenitis weidemeyerii BRh
Anthocharis scolymus BRh
Pieris rapae BRh (450 nm)
Colias erate BRh
Eurema hecabe BRh
Colias erate VRh1
Eurema hecabe VRh1
Pieris rapae VRh (420 nm)
Eurema hecabe VRh2
Colias erate VRh2
ILVAM Aliphatic/Hydrophobic
STNW Hydrophilic
PG Conformationally special
DE Negative
KRH Positive
Cysteine
FWY Aromatic
Helix 3
β-strands
Helix 5
Helix 6
Helix 7
B
Eat-BRh1 (λmax= 435 nm)
Eat-BRh2 (λmax= 500 nm)
Absorbance
Wavelength (nm)
C
F207
helix 5
I206
I120
helix 3
A116
G175
Y177
β-strands
D
helix 3
I120
Y177
A116
helix 5
5.1
3.2
2.6
E
A116S (440 nm)
BRh1
A116S/I120F (455 nm)
A116S/I120F/Y177F (475 nm)
Absorbance
Wavelength (nm)
F
Y177F
I120F
A116S
3.2
3.7
2.5
3.7
G
Y177F (514 nm)
Y177F/A116S (526 nm)
Y177F/G175S (515 nm)
Y177F/A116S/G175S (508 nm)
Absorbance
Wavelength (nm)
H
G175S
Y177F
A116S
6.0
8.6
5.2
2.5
5.2

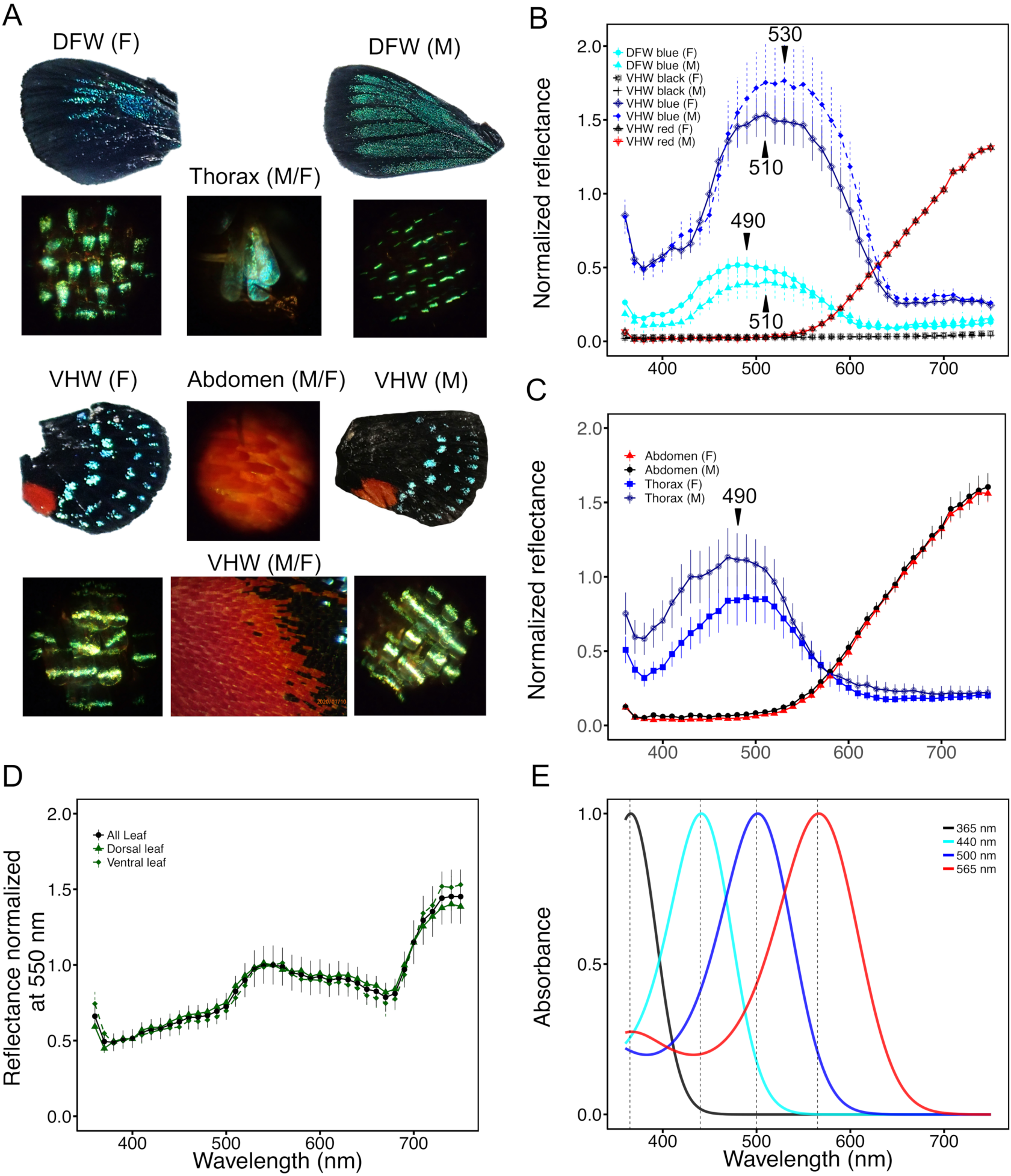
A
DFW (F)
DFW (M)
Thorax (M/F)
VHW (F)
Abdomen (M/F)
VHW (M)
VHW (M/F)
B
530
510
490
510
DFW blue (F)
DFW blue (M)
VHW black (F)
VHW black (M)
VHW blue (F)
VHW blue (M)
VHW red (F)
VHW red (M)
Normalized reflectance
C
490
Abdomen (F)
Abdomen (M)
Thorax (F)
Thorax (M)
Normalized reflectance
D
All Leaf
Dorsal leaf
Ventral leaf
Reflectance normalized at 550 nm
Wavelength (nm)
E
365 nm
440 nm
500 nm
565 nm
Absorbance
Wavelength (nm)